

Disclosing the preferential mercury chelation by SeCys containing peptides over their Cys analogues

*Mikel Bernabeu de Maria, Diego Tesauero, Filippo Prencipe, Michele Saviano, Luigi Messori, Christine Enjalbal, Ryszard Lobinski, Luisa Ronga **

Dr. Luisa Ronga, Dr. Ryszard Lobinski, Mikel Bernabeu De Maria-Pays de l'Adour, E2S UPPA, CNRS, IPREM, 64000 Pau, France.

Prof. D. Tesauero, Pr. F. Rossi- Department of Pharmacy and CIRPeB, Università degli Studi di Napoli Federico II, 49 80131 Naples, Italy.

Dr. Filippo Prencipe, Dr. Michele Saviano- Istituto di Cristallografia (IC), CNR, 70126 Caserta Italy.

Prof. Luigi Messori- Department of Chemistry, Università degli Studi di Firenze, 50019 Sesto Fiorentino, Italy

Prof. Christine Enjalbal- IBMM, Université de Montpellier, CNRS, ENSCM, UMR 5247, 34293 Montpellier Cedex 5, France.

Dr. Ryszard Lobinski- Warsaw University of Technology, 00-664 Warsaw, Poland.

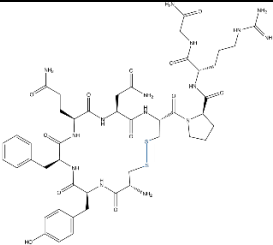
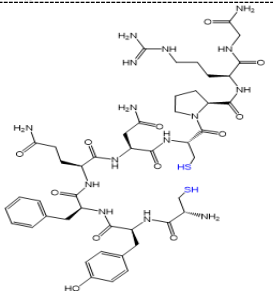
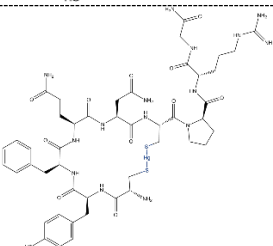
*Corresponding author E-mail: luisa.ronga@univ-pau.fr

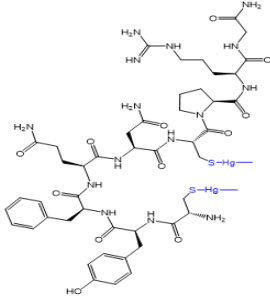
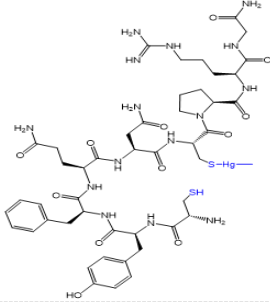
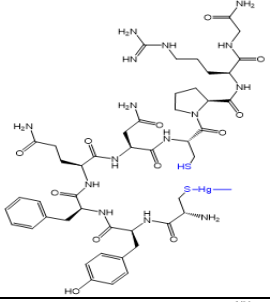
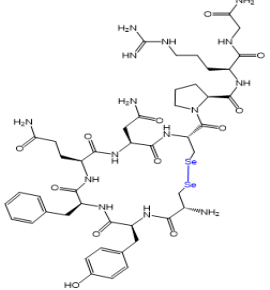
Table of Contents

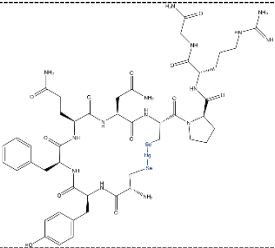
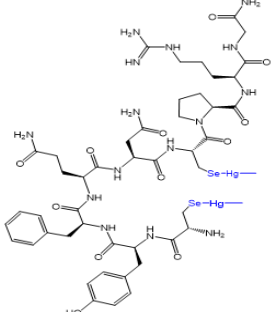
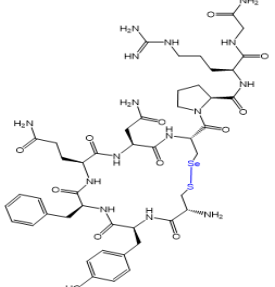
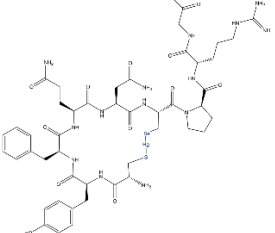
1. AVP PEPTIDES AND THEIR MERCURY ADDUCTS IDENTIFIED BY MS	3
1.1. Table S1. AVP peptides and their Hg adducts identified by mass spectrometry after incubation of the peptides with HgCl ₂ or CH ₃ HgCl or Hg ₂ Cl ₂	3
1.2. Comparison of theoretical and experimental isotopic patterns	7
2. IMAGES OF RESULTS	12
2.1. Characterization of synthetic products	12
2.2. AVP peptides reactivity with CH ₃ HgCl	15
2.4. AVP peptides reactivity with HgCl ₂	18
2.5. AVP peptides reactivity with Hg ₂ Cl ₂	21
2.6. Competitive reactivity study	23
2.7. MS/MS of Hg-peptide adducts	25

1. AVP PEPTIDES AND THEIR MERCURY ADDUCTS IDENTIFIED BY MS

1.1. Table S1. AVP peptides and their Hg adducts identified by mass spectrometry after incubation of the peptides with HgCl₂ or CH₃HgCl or Hg₂Cl₂.

Peptide	Chemical structure	Formula	Theoretical monoisotopic mass (Da)	Experimental mass of the most abundant isotope (Se ^{79.9160} and Hg ^{201.9701}) (Da)	Observed most abundant ions m/z	
					z=1 [M+H] ⁺	z=2 [M+2H] ²⁺
AVP		C ₄₆ H ₆₅ N ₁₅ O ₁₂ S ₂	1083.4373	1083.4368	1084.4441	542.7257
Reduced AVP		C ₄₆ H ₆₇ N ₁₅ O ₁₂ S ₂	1085.4530	1085.4525	1086.4598	543.7340
Hg-bridged AVP ^a		C ₄₆ H ₆₅ HgN ₁₅ O ₁₂ S ₂	1285.4079	1285.4090	1286.4163	643.7114

Bis-metallated AVP ^b		$C_{48}H_{71}Hg_2N_{15}O_{12}S_2$	1517.4255	1515.4236	1516.4309	758.7191
Monometallated AVP ^b		$C_{47}H_{69}HgN_{15}O_{12}S_2$	1301.4392	1301.4525	1302.4598	651.7266
Monometallated AVP' ^b		$C_{47}H_{69}HgN_{15}O_{12}S_2$	1301.4392	1301.4525	1302.4598	651.7266
(Se-Se)-AVP		$C_{46}H_{65}N_{15}O_{12}Se_2$	1179.3262	1179.3266	1180.3339	590.6707

Hg-bridged (Se-Se)-AVP ^a		$C_{46}H_{65}HgN_{15}O_{12}Se_2$	1381.2968	1379.2978	1380.3051	690.6556
Bis-metallated (Se-Se)-AVP ^b		$C_{48}H_{71}Hg_2N_{15}O_{12}Se_2$	1613.3144	1609.3123	1610.3196	805.6631
(S-Se)-AVP		$C_{46}H_{65}N_{15}O_{12}SSe$	1131.3817	1131.3804	1132.3877	566.6975
Hg-bridged (S-Se)-AVP ^a		$C_{46}H_{65}HgN_{15}O_{12}SSe$	1333.3524	1331.3526	1332.3599	666.6826

Bis-metallated (S-Se)-AVP ^b		$C_{48}H_{71}Hg_2N_{15}O_{12}S_2Se$	1565.3700	1563.3493	1564.3566	782.6912
Monometallated (S-Se)-AVP ^b		$C_{47}H_{69}HgN_{15}O_{12}S_2Se$	1349.3842	1347.3635	1348.3708	674.7001
Monometallated (S-Se)-AVP ^{a, b}		$C_{47}H_{69}HgN_{15}O_{12}S_2Se$	1349.3837	1347.3635	1348.3708	674.7001

^a Formed with $HgCl_2$, CH_3HgCl and Hg_2Cl_2 .

^b Formed only with CH_3HgCl .

1.2. Comparison of theoretical and experimental isotopic patterns

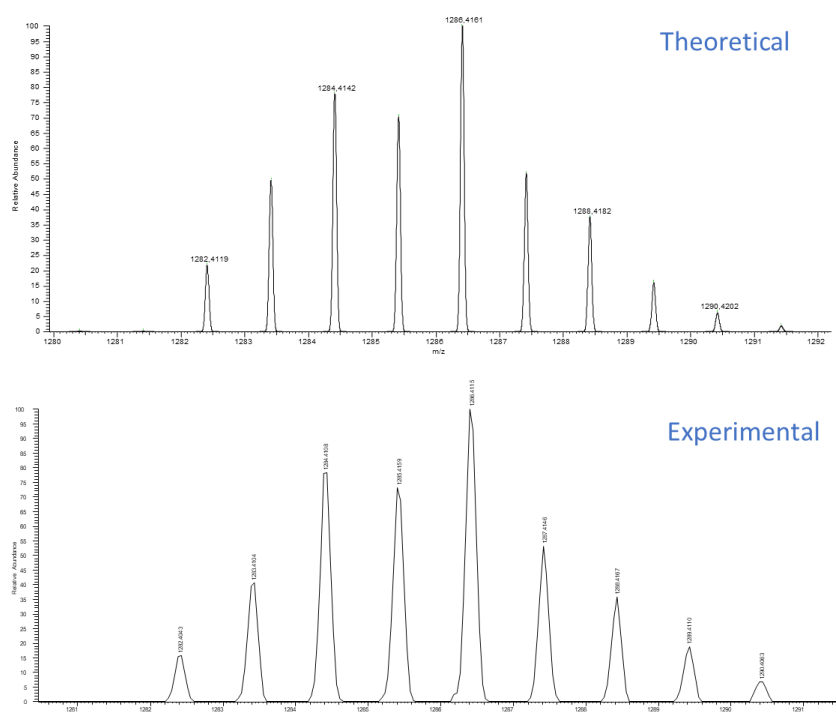


Figure S1. Hg-bridged AVP, 1286.4161 ion (m/z): comparison of experimental and theoretical (calculated as $[M+H]^+$) isotopic patterns.

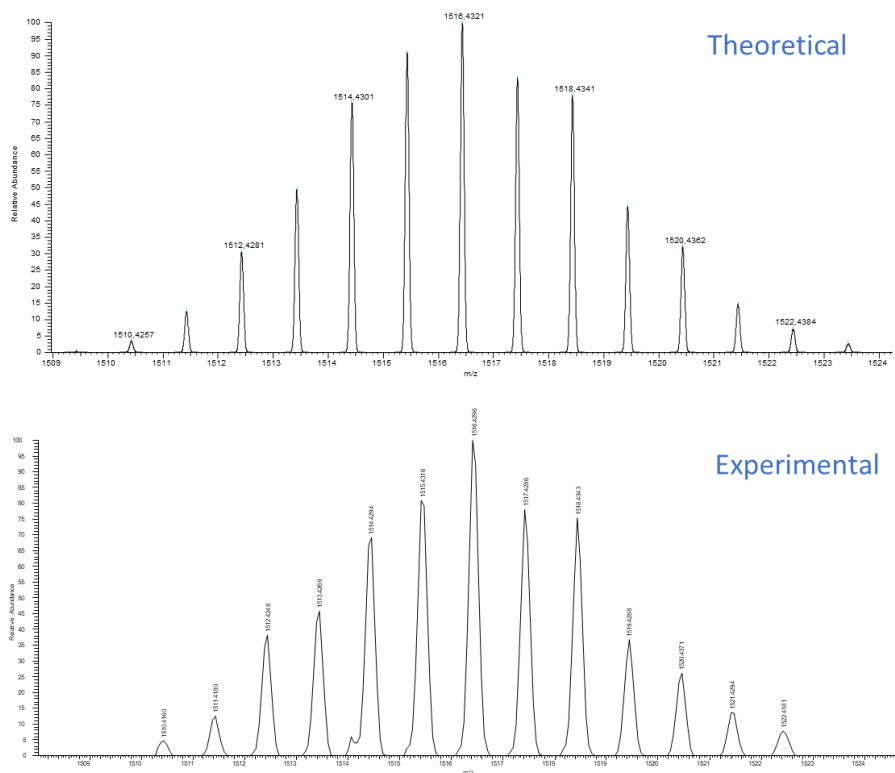


Figure S2. Bis-metallated AVP, 1516.4321 ion (m/z): comparison of experimental and theoretical (calculated as $[M+H]^+$) isotopic patterns.

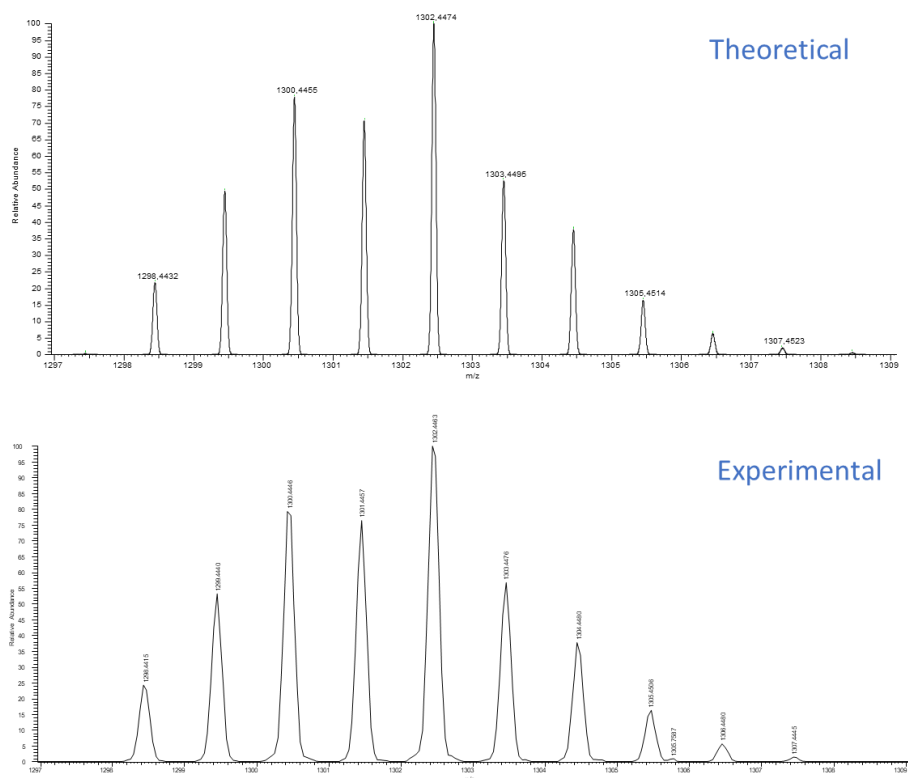


Figure S3. Monometallated AVP, 1302.4474 ion (m/z): comparison of experimental and theoretical (calculated as $[M+H]^+$) isotopic patterns.

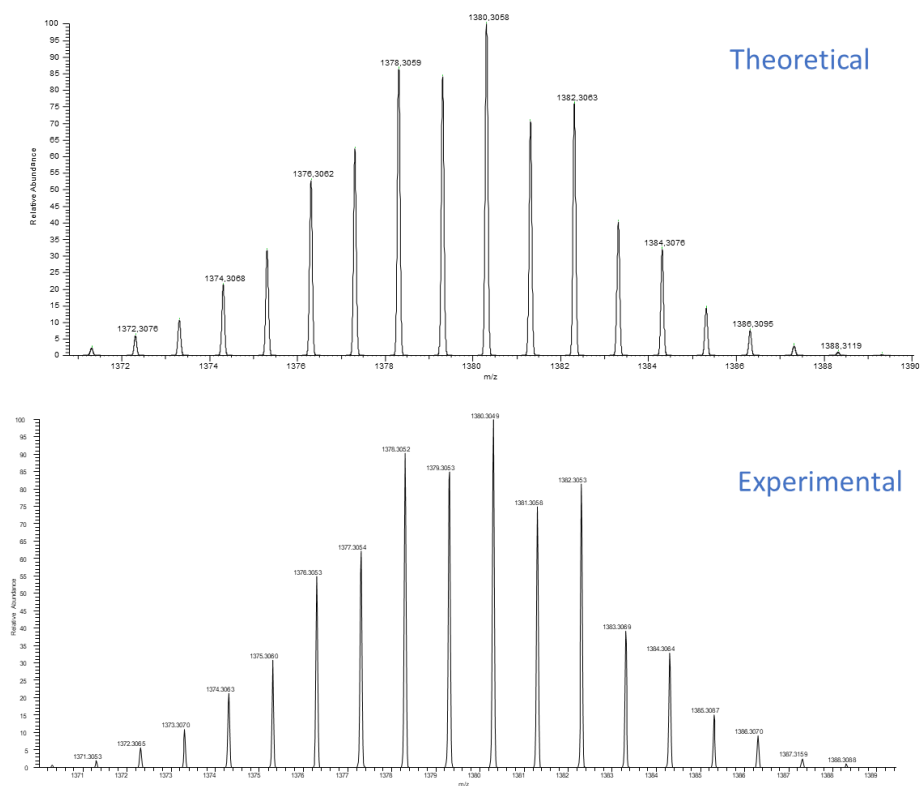


Figure S4. Hg-bridged (Se-Se)-AVP, 1380.3058 ion (m/z): comparison of experimental and theoretical (calculated as $[M+H]^+$) isotopic patterns.

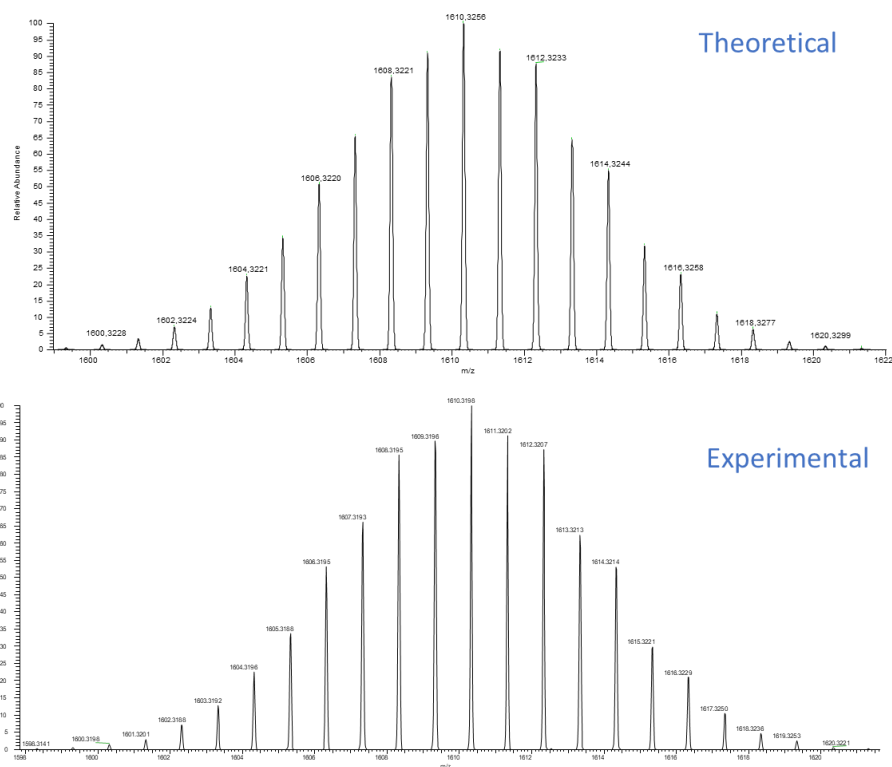


Figure S5. Bis-metallated (Se-Se)-AVP, 1610.3256 ion (m/z): comparison of experimental and theoretical (calculated as $[M+H]^+$) isotopic patterns.

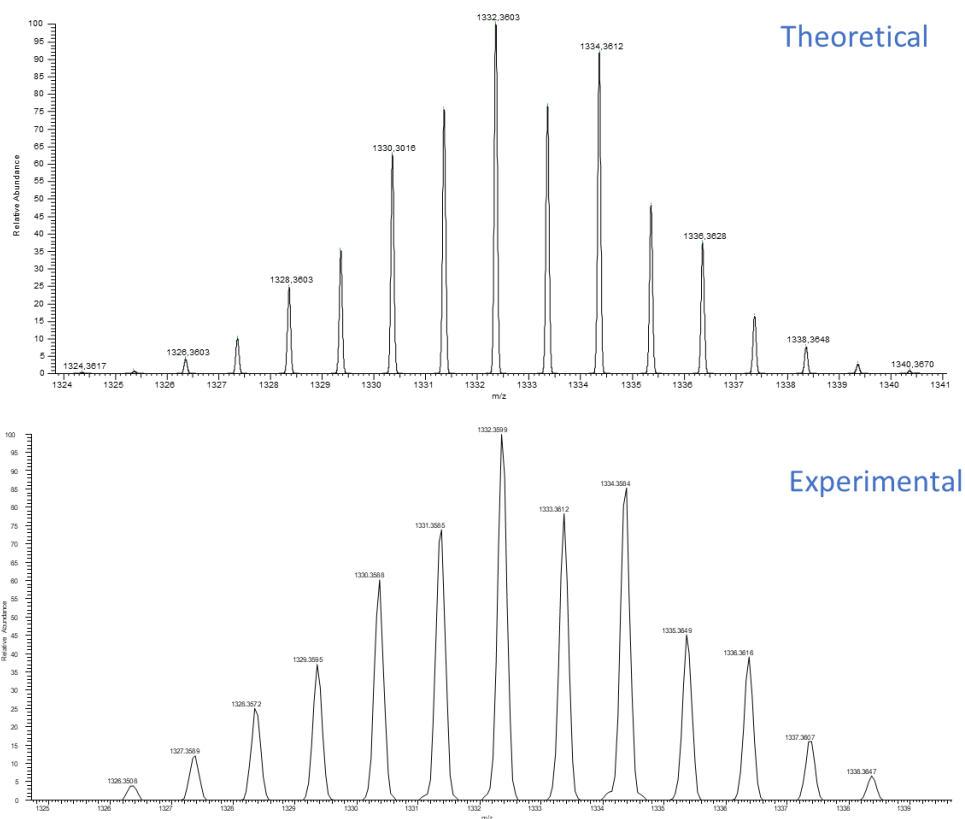


Figure S6. Hg-bridged (S-Se)-AVP, 1332.3603 ion (m/z): comparison of experimental and theoretical (calculated as $[M+H]^+$) isotopic patterns.

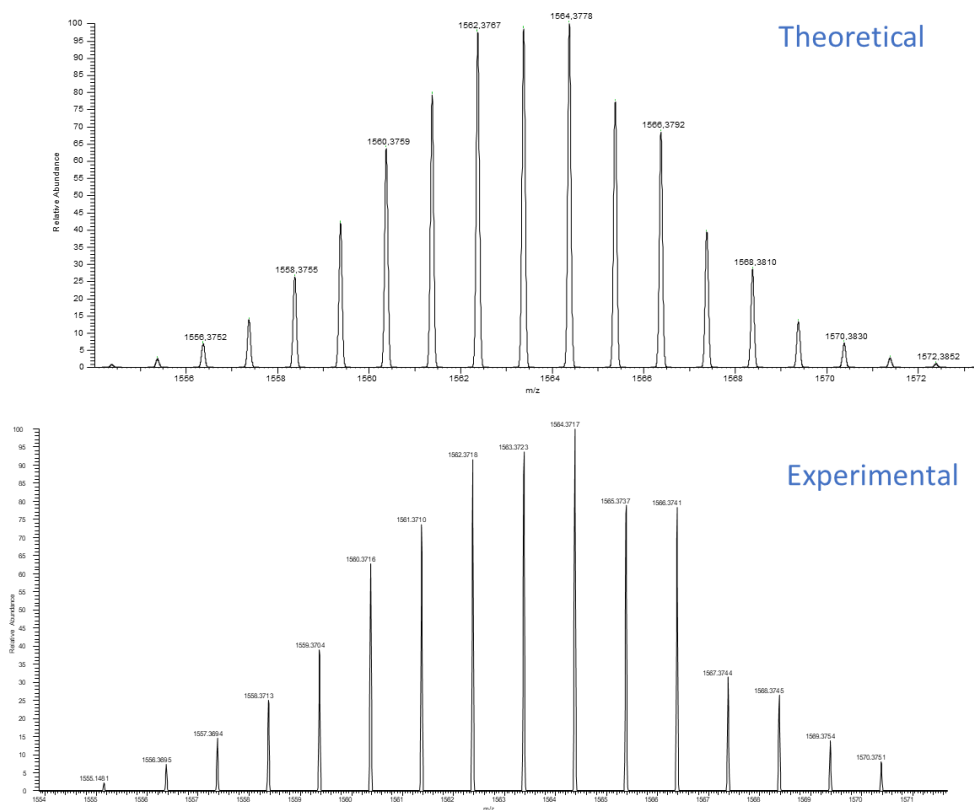


Figure S7. Bis-metallated (S-Se)-AVP, 1564.3778 ion (m/z): comparison of experimental and theoretical (calculated as $[M+H]^+$) isotopic patterns.

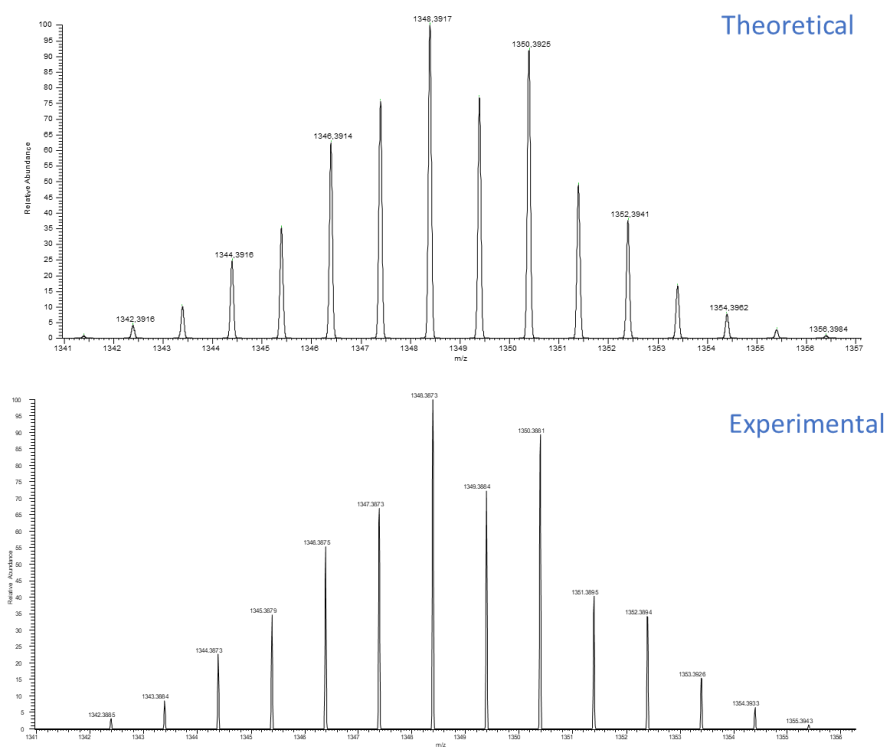


Figure S8. Monometallated (S-Se)-AVP, 1348.3917 ion (m/z): comparison of experimental and theoretical (calculated as $[M+H]^+$) isotopic patterns.

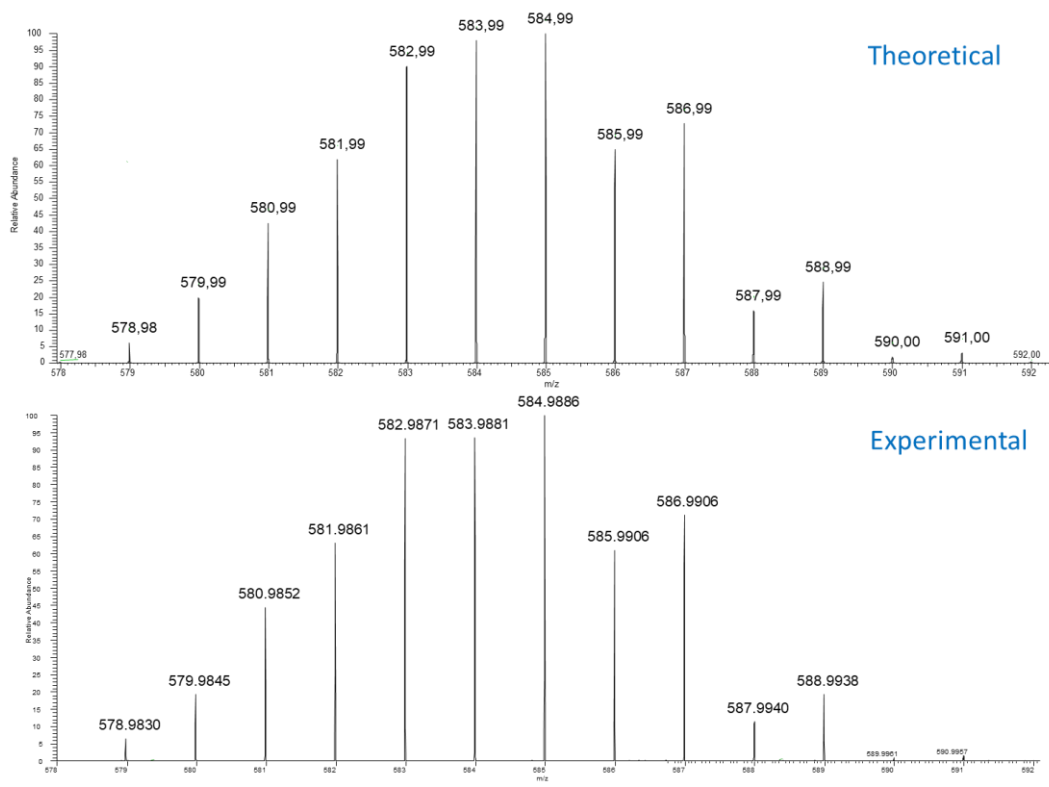


Figure S9. CH₃Hg-DTT adducts: [DTT-2H+2CH₃Hg+H]⁺, 584.9886 m/z: comparison of experimental and theoretical (calculated as [M+H]⁺) isotopic patterns.

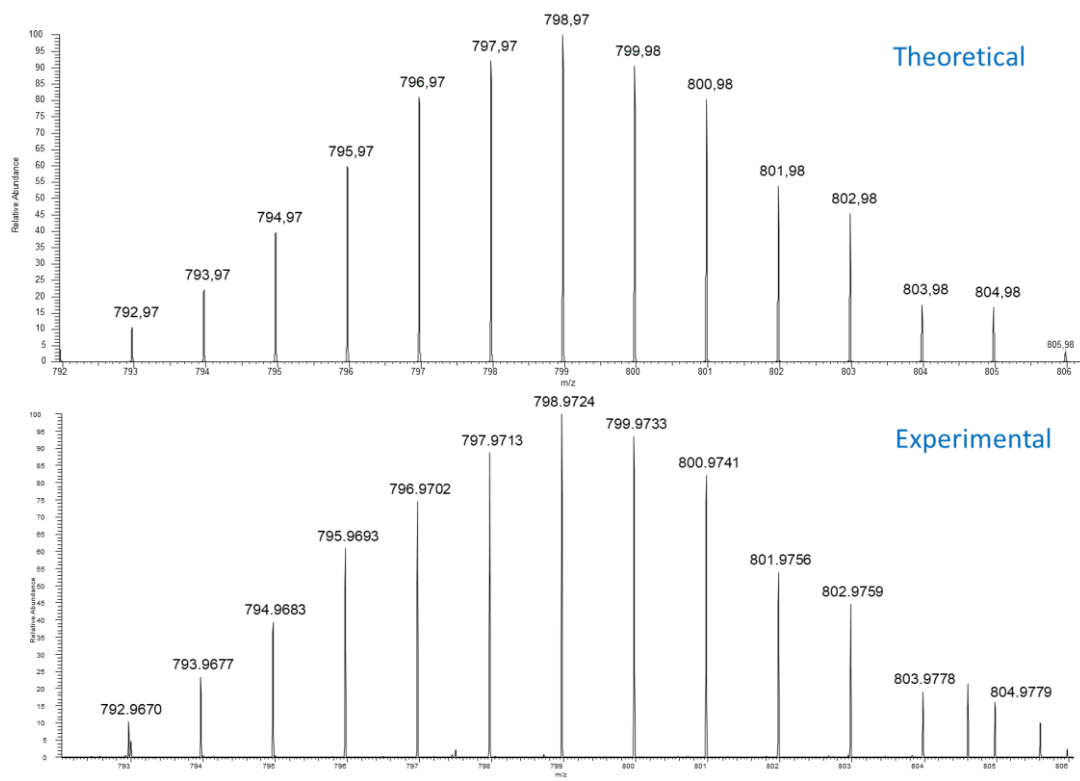


Figure S10. CH₃Hg-DTT adducts: [DTT-3H+3CH₃Hg+H]⁺, 798.9724 m/z: comparison of experimental and theoretical (calculated as [M+H]⁺) isotopic patterns.

2. IMAGES OF RESULTS

2.1. Characterization of synthetic products

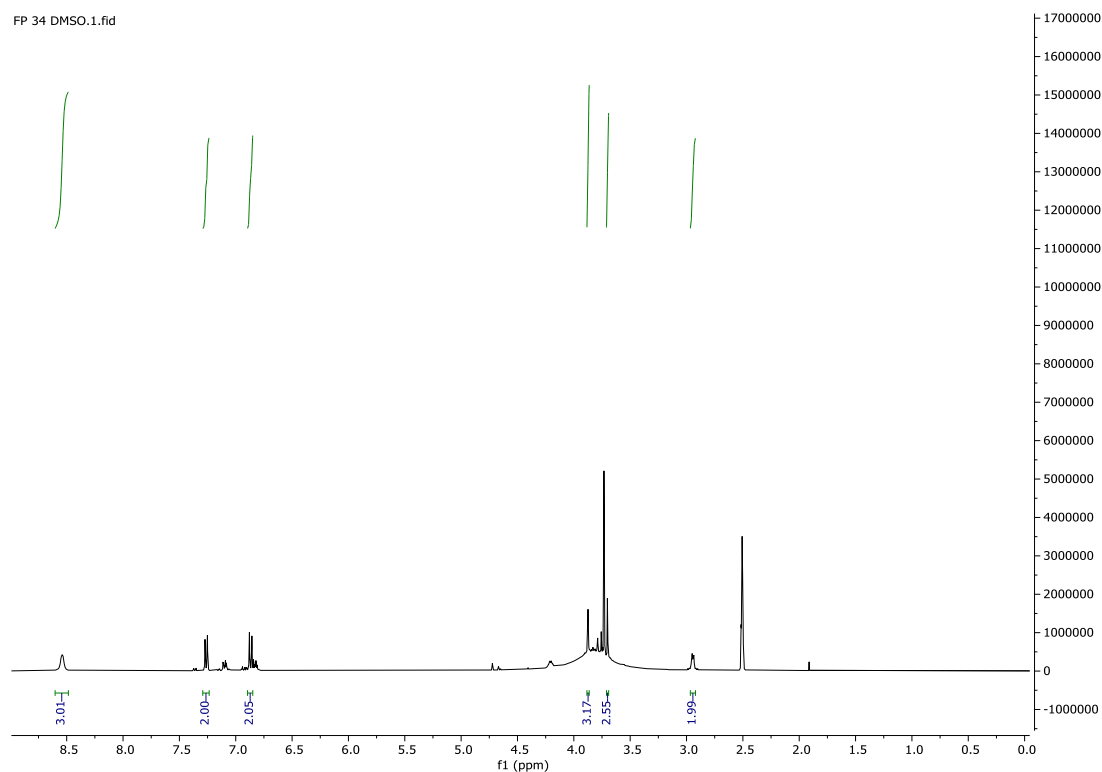


Figure S11. ^1H NMR of SeCys(MBzl) in $(\text{CD}_3)_2\text{SO}$

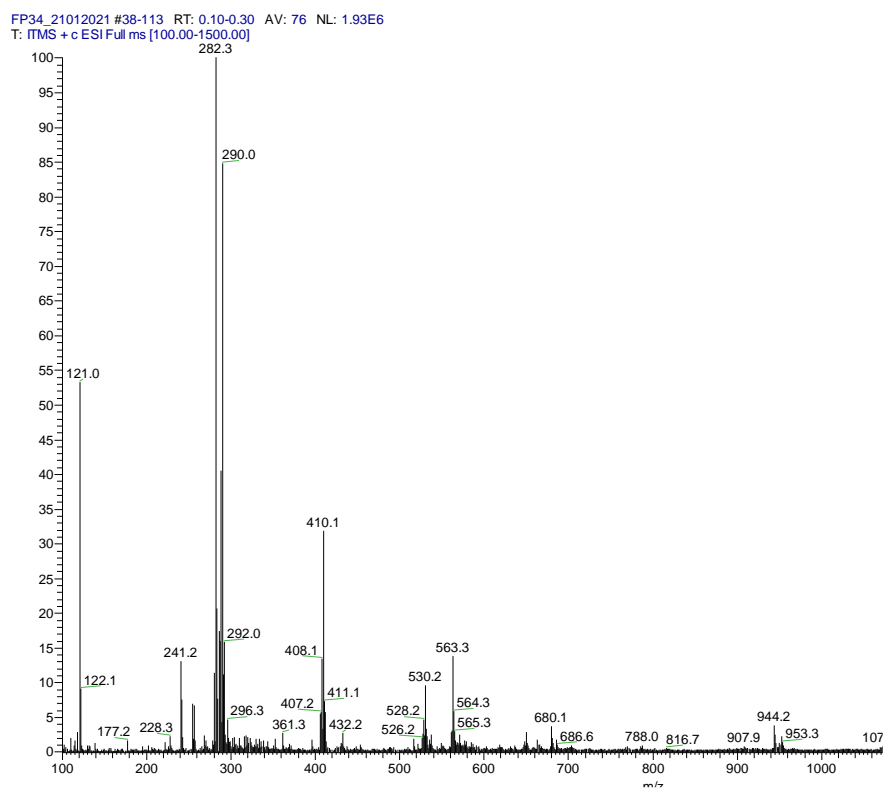


Figure S12. ESI-MS of SeCys(MBzl)

FP 37 DMSO

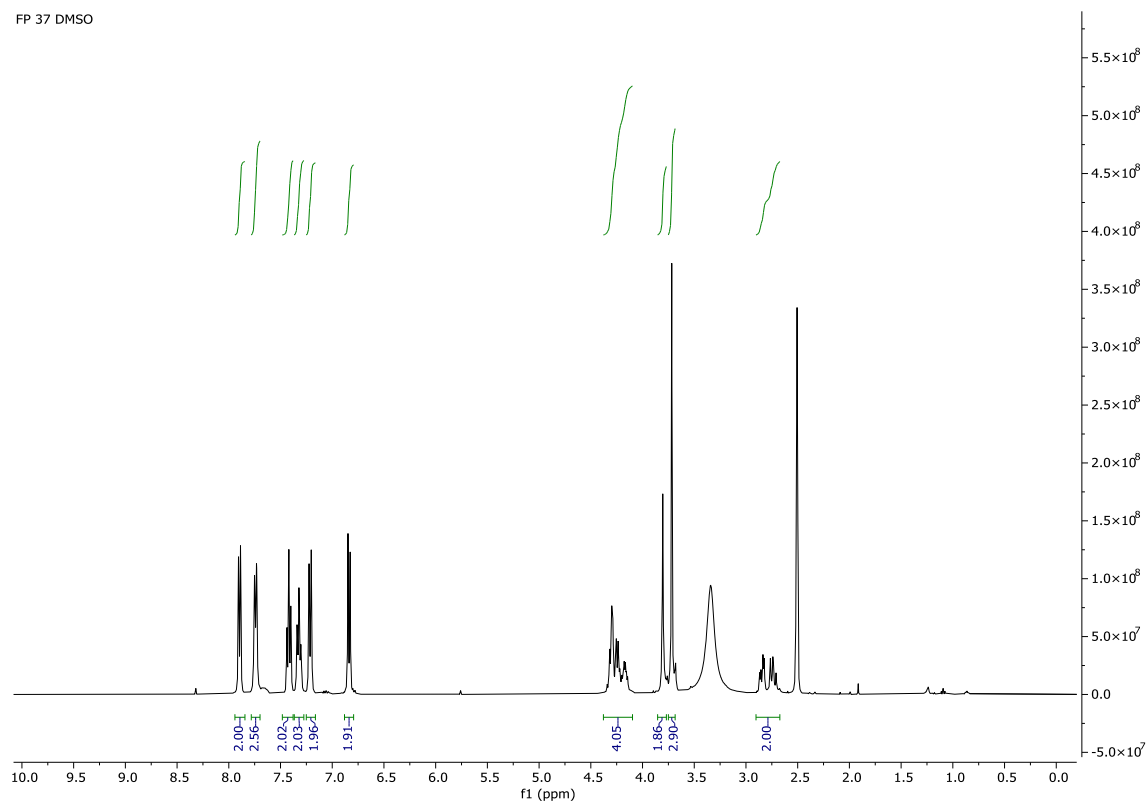


Figure S13. ^1H NMR of Fmoc-Sec(MBzl)

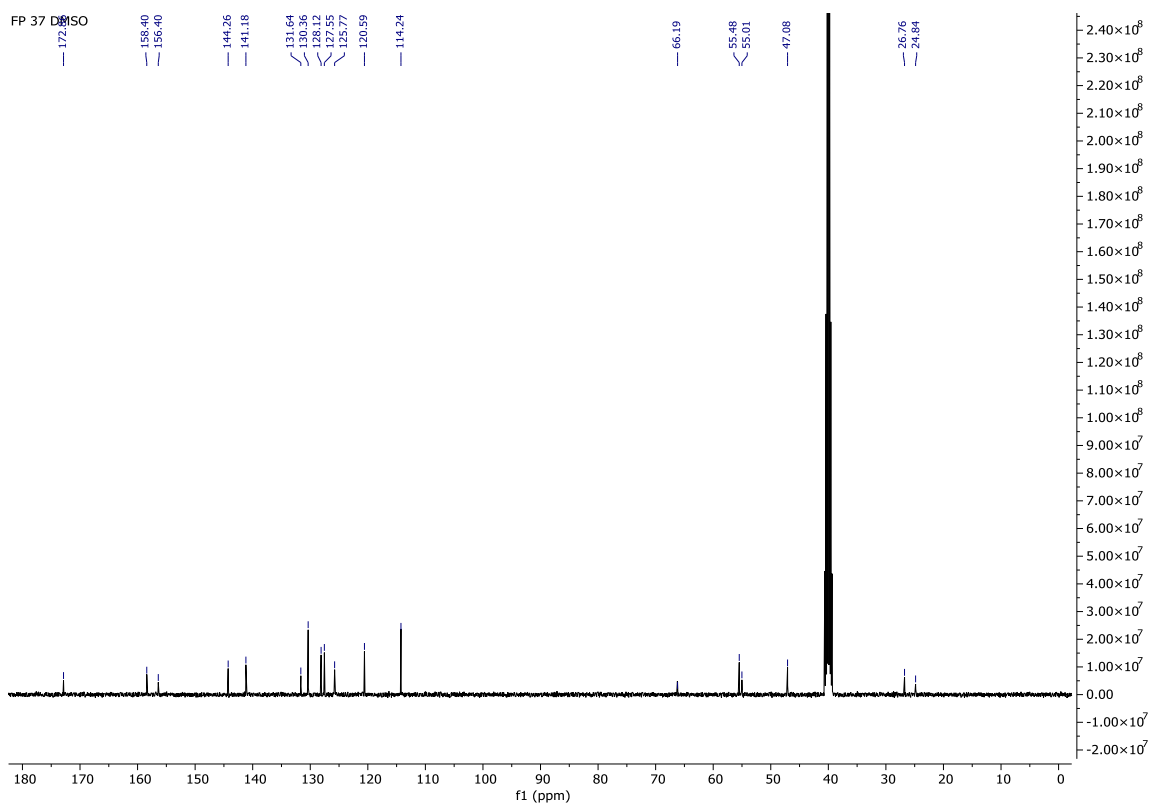


Figure S14. ^{13}C NMR of Fmoc-Sec(MBzl)

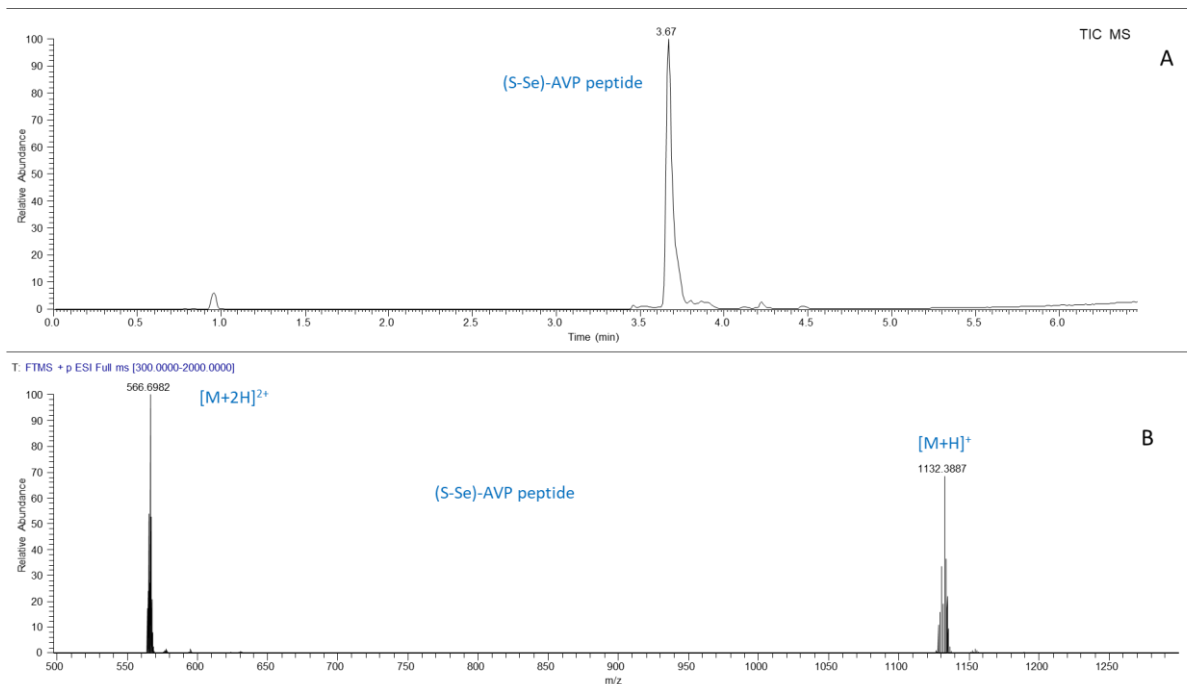


Figure S15. LC-MS of (S-Se)-AVP. **(A)** TIC. **(B)** MS spectrum of peak at $t_R = 3.67$ min.

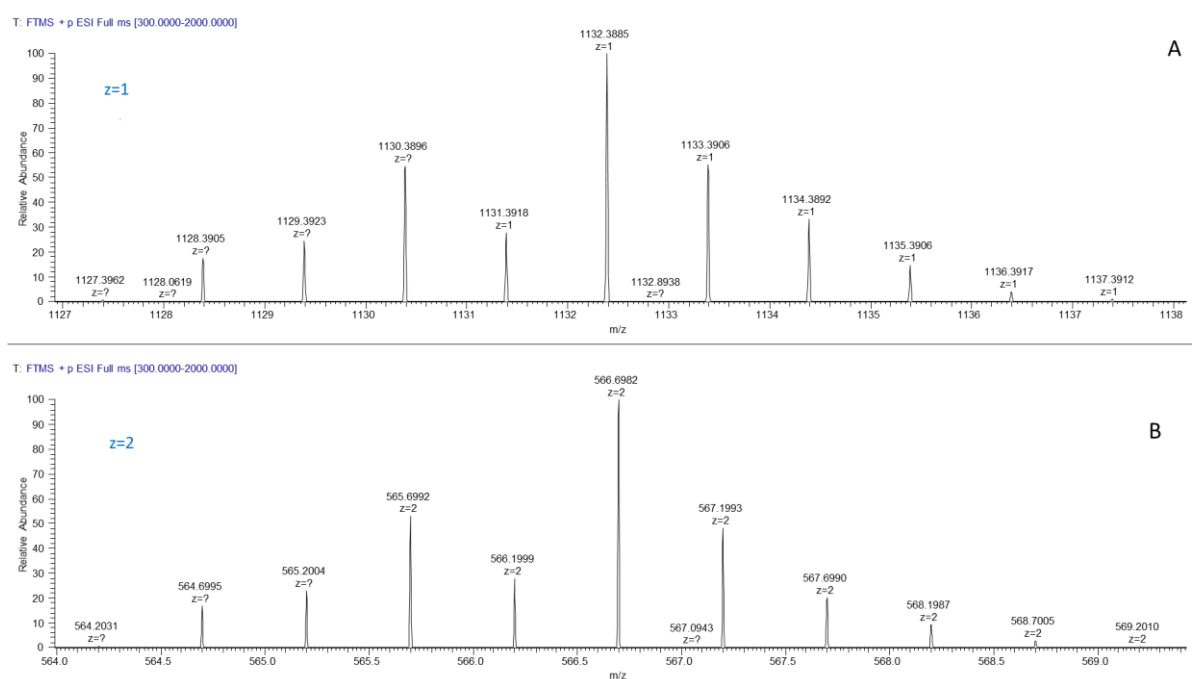


Figure S16. **(A)** MS isotopic pattern of (S-Se)-AVP for the mono-charged (m/z 1132.3885) and **(B)** di-charged ion (m/z 566.6982).

2.2. AVP peptides reactivity with CH₃HgCl

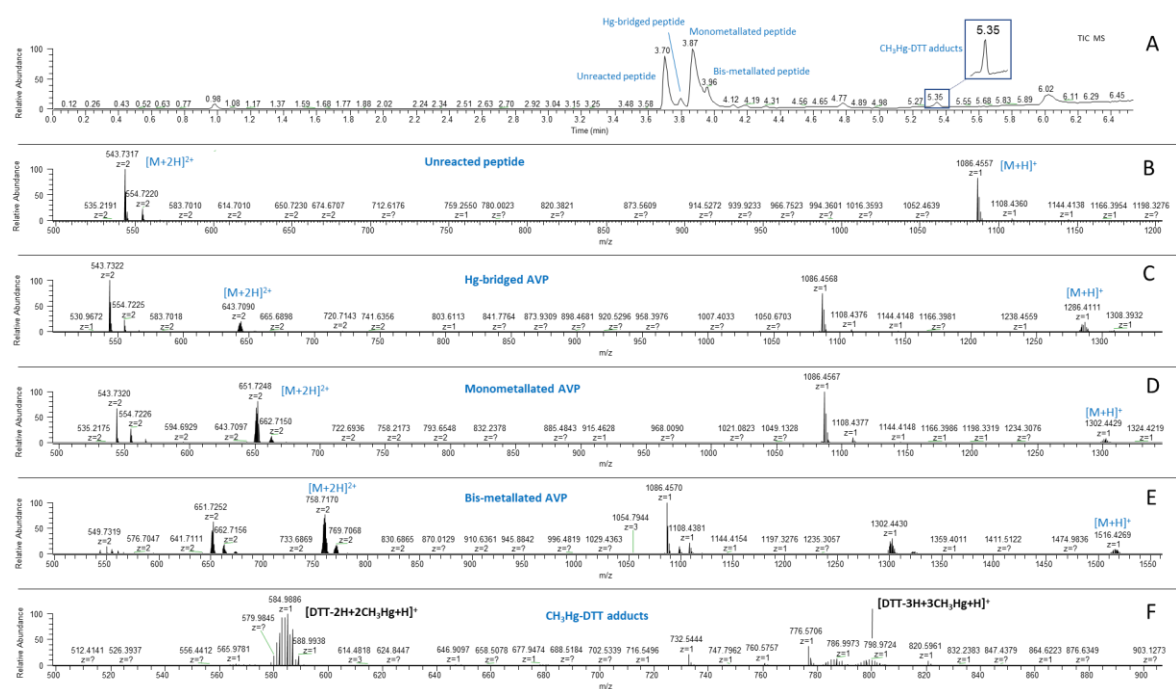


Figure S17. LC-MS of AVP incubated (18 h) with CH₃HgCl (2 equiv) at 37 °C in presence of DTT. (A) TIC. (B) MS spectrum of peak at $t_R = 3.70$ min. (C) MS spectrum of peak at $t_R = 3.80$ min. (D) MS spectrum of peak at $t_R = 3.87$ min. (E) MS spectrum of peak at $t_R = 3.96$ min (F) MS spectrum of peak at $t_R = 5.35$ min.

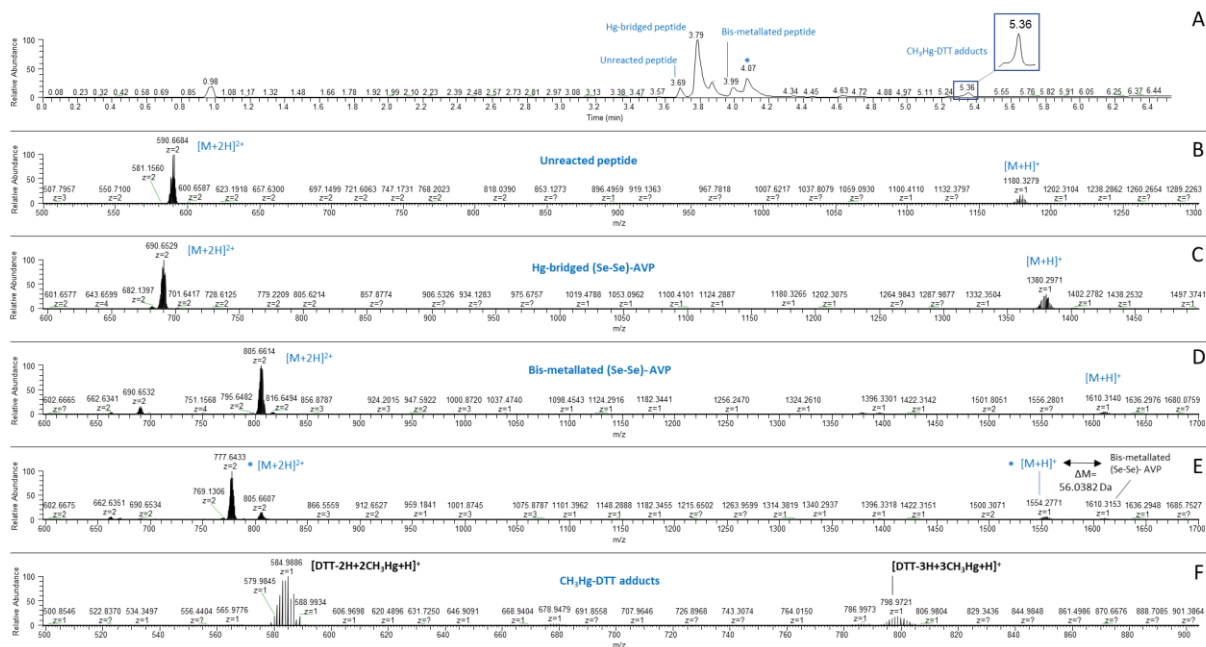


Figure S18. LC-MS of (Se-Se)-AVP incubated 18 h with CH₃HgCl (1 equiv) at 37 °C in presence of DTT. (A) TIC. (B) MS spectrum of peak at $t_R = 3.69$ min. (C) MS spectrum of peak at $t_R = 3.79$ min. (D) MS spectrum of peak at $t_R = 3.99$ min. (E) MS spectrum of peak at $t_R = 4.07$ min. (F) MS spectrum of peak at $t_R = 5.36$ min.

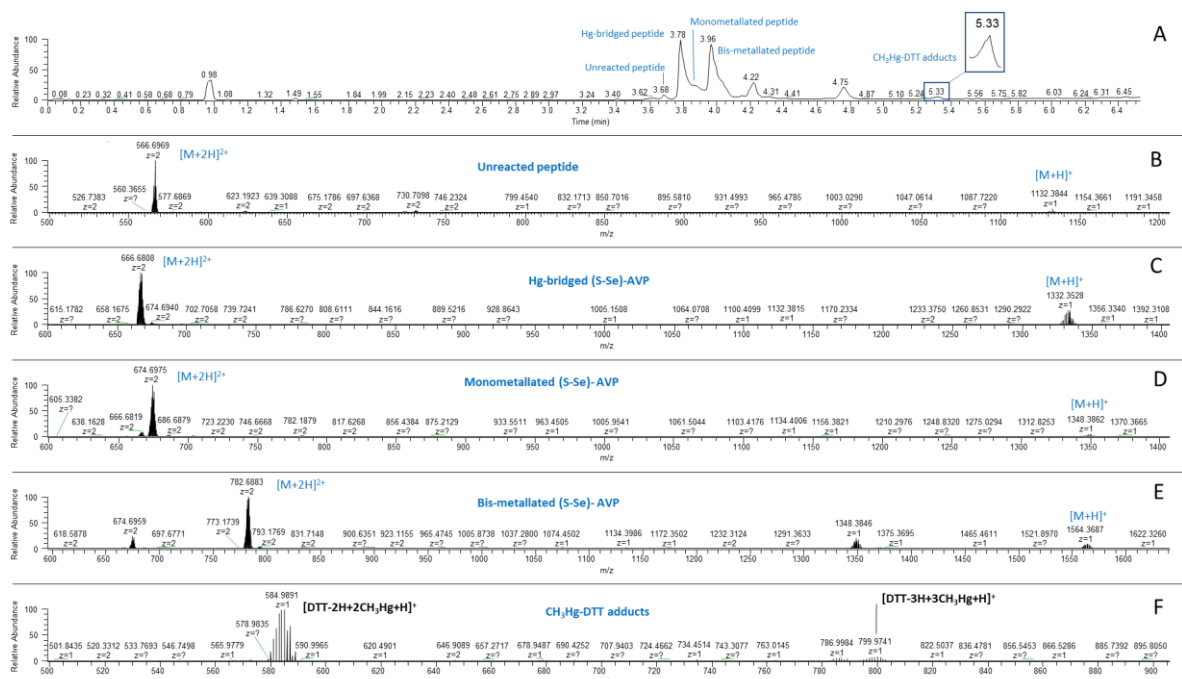


Figure S19. LC-MS of (S-Se)-AVP incubated 3 h with CH_3HgCl (1 equiv) at 37°C in presence of DTT. **(A)** TIC. **(B)** MS spectrum of peak at $t_R = 3.68$ min. **(C)** MS spectrum of peak at $t_R = 3.78$ min. **(D)** MS spectrum of peak at $t_R = 3.86$ min. **(E)** MS spectrum of peak at $t_R = 3.96$ min. **(F)** MS spectrum of peak at $t_R = 5.33$ min.

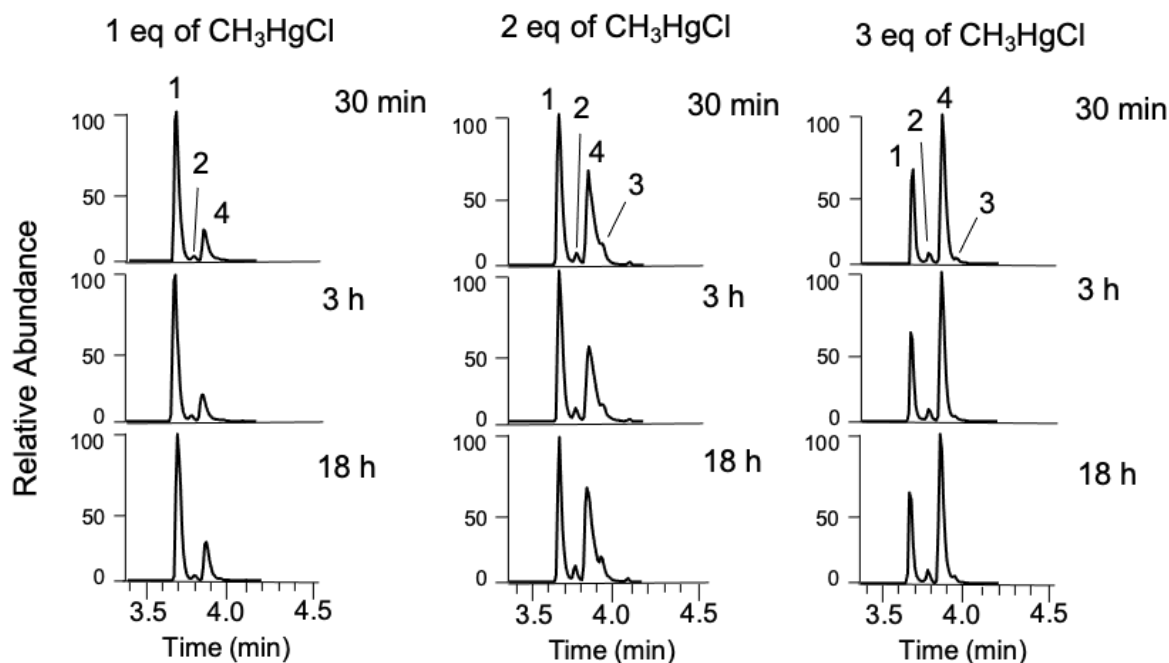


Figure S20. LC-MS of AVP incubated with 1, 2 and 3 equiv of CH_3HgCl at 37°C in presence of DTT during 30 min, 3 h and 18 h. XIC of ions m/z 543.73 (**1** unreacted peptide, $t_R=3.68$), 643.74 (**2** Hg-bridged peptide, $t_R=3.80$), 758.72 (**3** bis-metallated peptide, $t_R=3.86$) and 651.73 (**4** monometallated peptide, $t_R=3.93$)

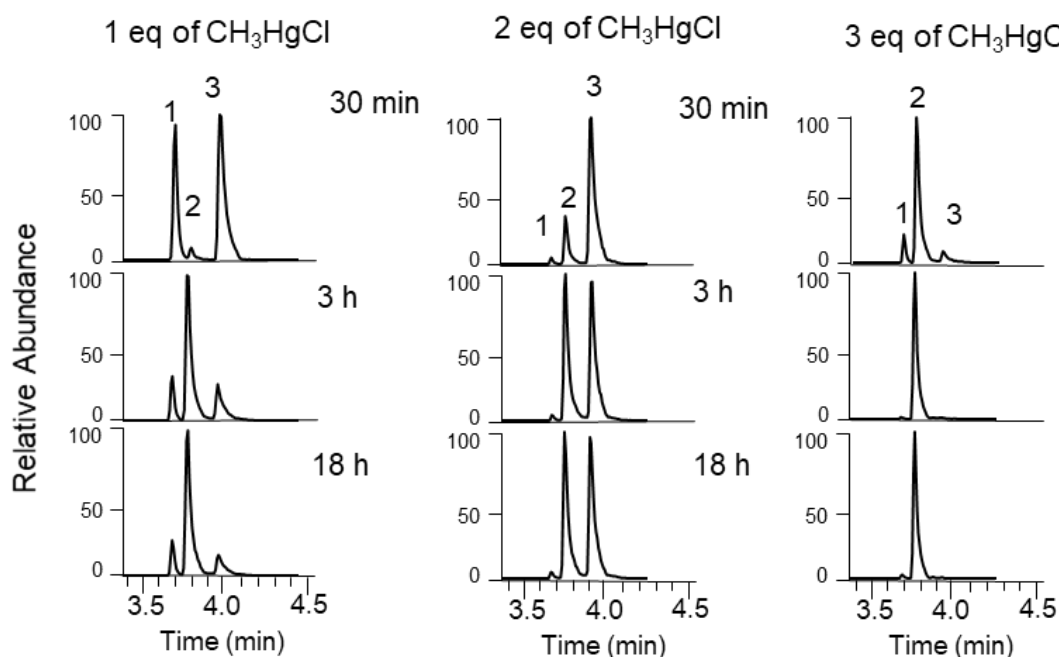


Figure S21. LC-MS of (Se-Se)-AVP incubated with 1, 2 or 3 equiv of CH_3HgCl at 37°C in presence of DTT during 30 min, 3 h and 18 h. XIC of ions m/z 590.67 (**1** unreacted peptide, $t_R=3.69$), 690.65 (**2** Hg-bridged peptide, $t_R=3.79$) and 805.66 (**3** bis-metallated peptide, $t_R=3.99$).

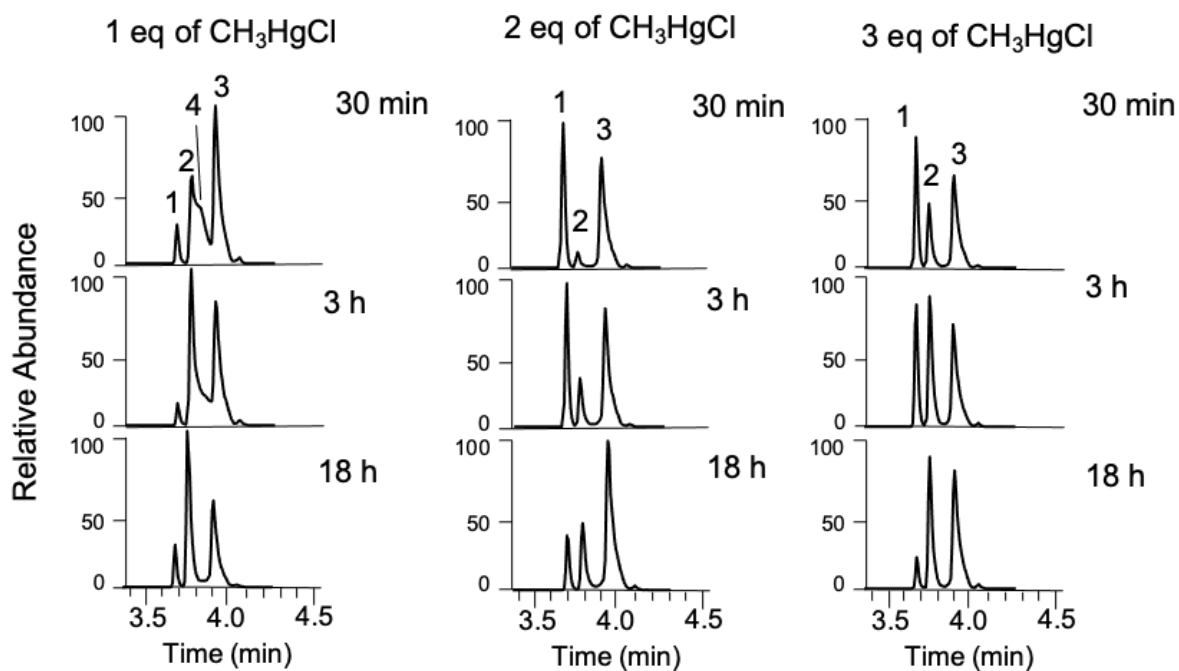


Figure S22. LC-MS of (S-Se)-AVP incubated with 1, 2 or 3 equiv of CH_3HgCl at 37°C in presence of DTT during 30 min, 3 h and 18 h. XIC of ions m/z 566.70 (**1** unreacted peptide, $t_R=3.68$ min), 666.68 (**2** Hg-bridged peptide, $t_R=3.79$ min), 782.69 (**3** bis-metallated peptide, $t_R=3.96$ min) and 674,.70 (**4** monometallated peptide, $t_R=3.83$ min).

2.4. AVP peptides reactivity with HgCl₂

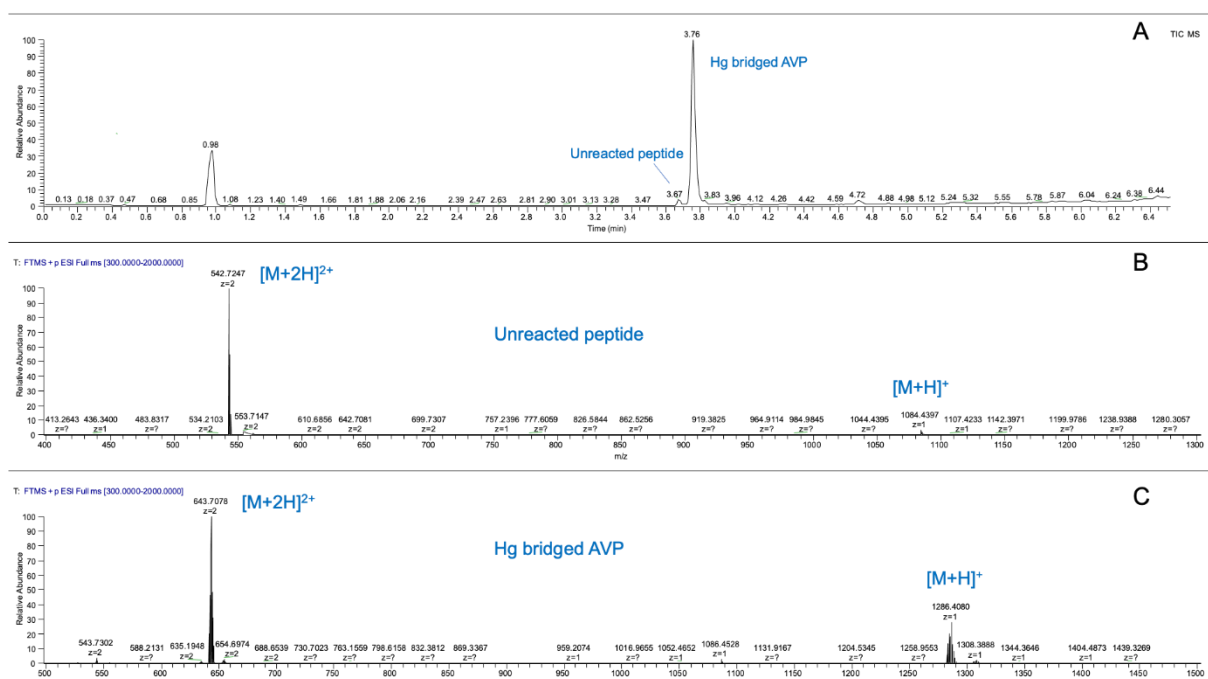


Figure S23. LC-MS of AVP incubated with 1 equiv of HgCl₂ at 37 °C in presence of DTT during 30 min, which is representative of AVP incubated with 1, 2 or 3 equiv of HgCl₂ at 37 °C in presence of DTT during 30 min, 3 h and 18 h. **(A)** TIC. **(B)** MS spectrum of peak at t_R = 3.67 min. **(C)** MS spectrum of peak at t_R=3.76 min.

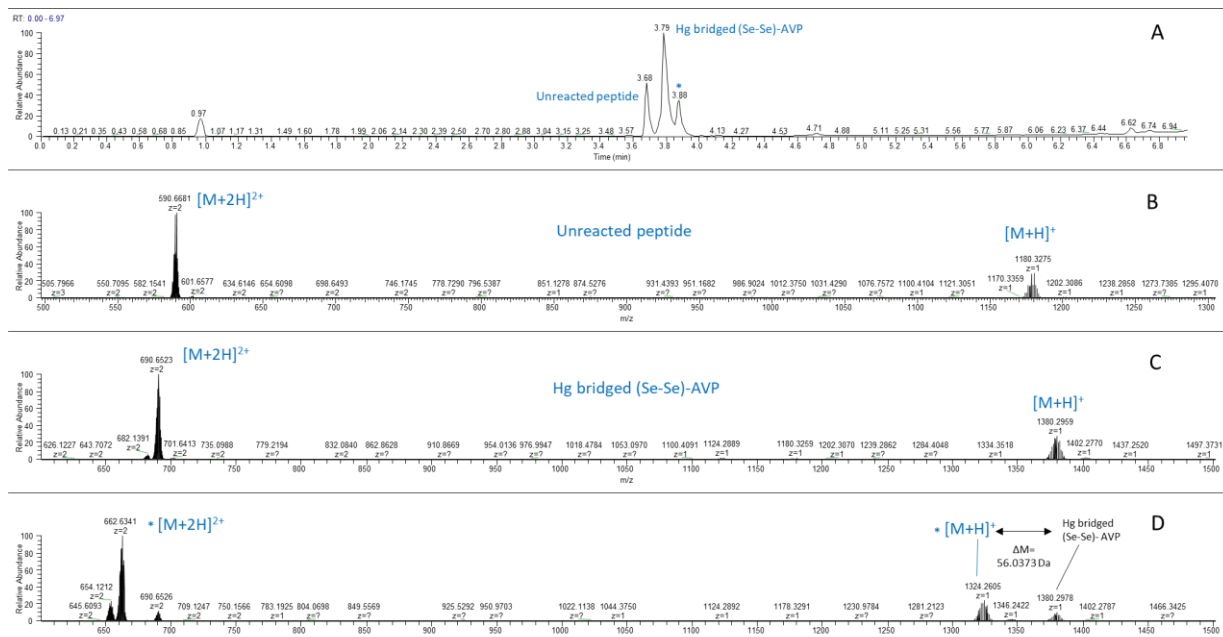


Figure S24. LC-MS of (Se-Se)-AVP incubated 18 h with HgCl₂ (2 equiv) at 37 °C in presence of DTT. **(A)** TIC. **(B)** MS spectrum of peak at t_R = 3.68 min. **(C)** MS spectrum of peak at t_R = 3.79 min. **(D)** MS spectrum of peak at t_R = 3.88 min.

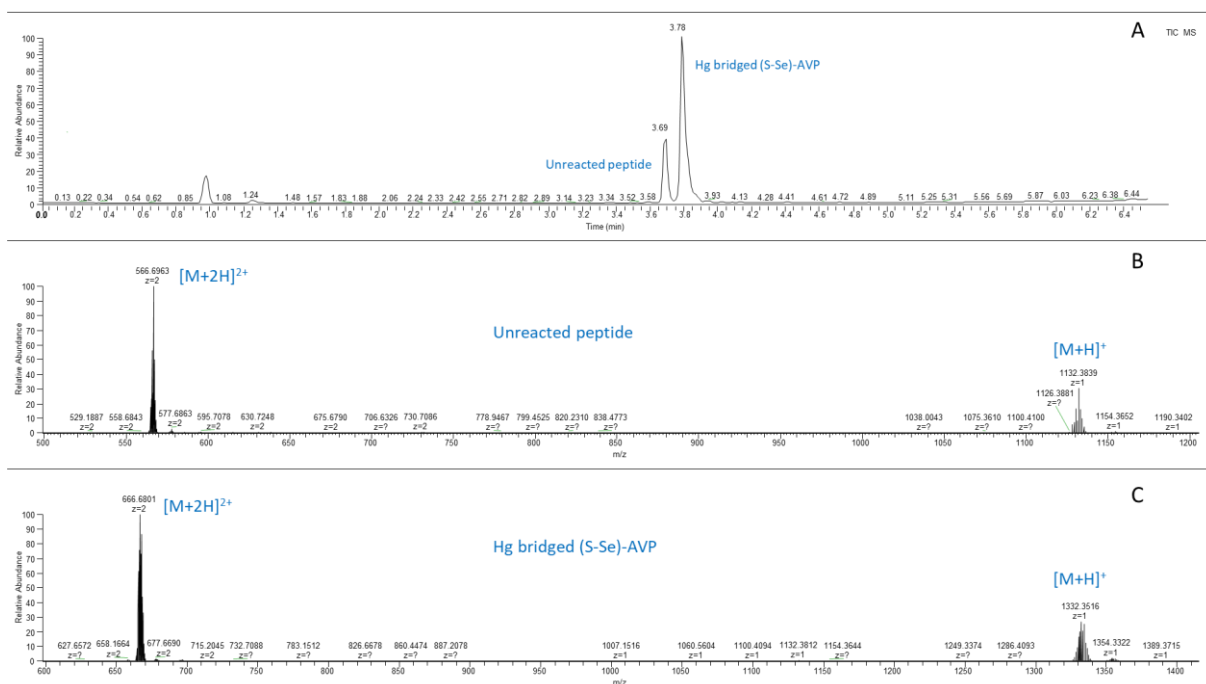


Figure S25. LC-MS of (S-Se)-AVP incubated 18 h with HgCl_2 (2 equiv) at 37 °C in presence of DTT. (A) TIC. (B) MS spectrum of peak at $t_R = 3.69$ min. (C) MS spectrum of peak at $t_R = 3.78$ min.

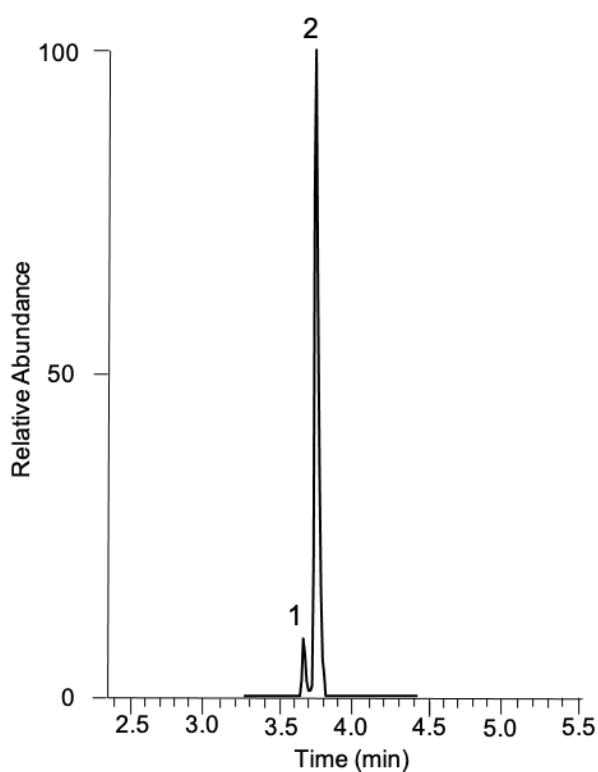


Figure S26. LC-MS of AVP incubated with 1 equiv of HgCl_2 at 37 °C in presence of DTT during 30 min, which is representative of AVP incubated with 1, 2 or 3 equiv of HgCl_2 at 37 °C in presence of DTT during 30 min, 3 h and 18 h. XIC of ions m/z 542,72 (**1** unreacted peptide, $t_R=3.67$ min) and 643,71 (**2** Hg-bridged peptide, $t_R=3.76$ min).

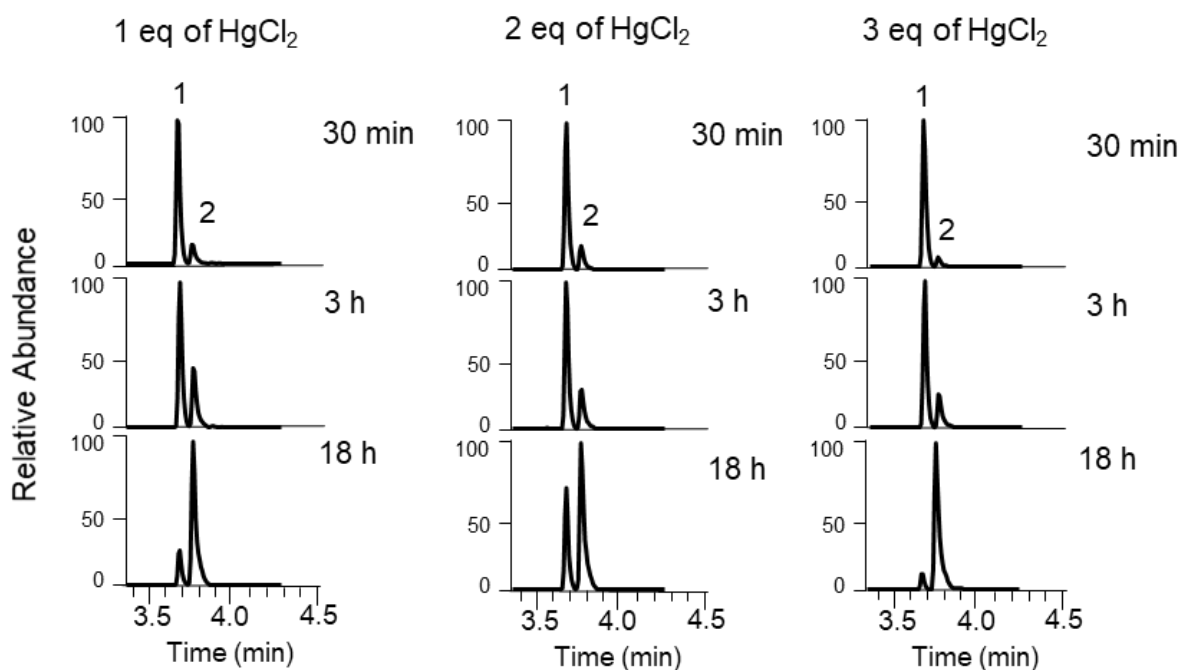


Figure S27. LC-MS of (Se-Se)-AVP incubated with 1, 2 or 3 equiv. of HgCl₂ at 37 °C in presence of DTT during 30 min, 3 h and 18 h. XIC of ions m/z 590.67 (1 unreacted peptide, t_R=3.68 min) and 690.65 (2 Hg-bridged peptide, t_R=3.79 min).

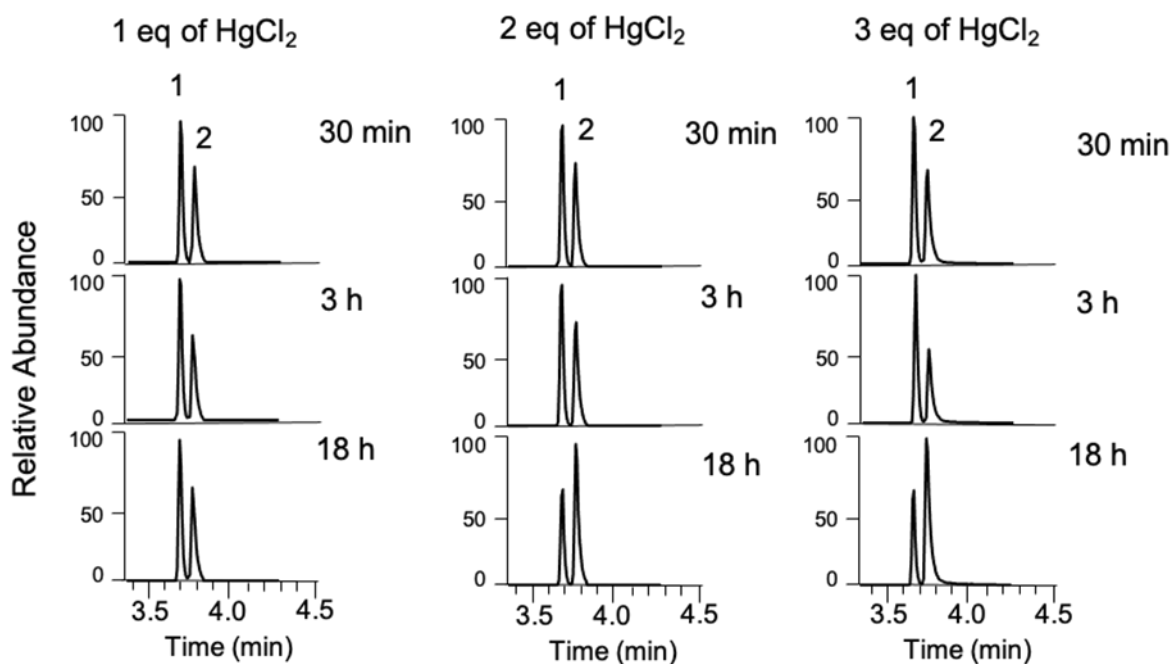


Figure S28. LC-MS of (S-Se)-AVP incubated with 1, 2 or 3 equiv of HgCl₂ at 37 °C in presence of DTT during 30 min, 3 h and 18 h. XIC of ions m/z 566.70 (1 unreacted peptide, t_R=3.69 min) and 666.68 (2 Hg-bridged peptide, t_R=3.78 min).

2.5. AVP peptides reactivity with Hg₂Cl₂

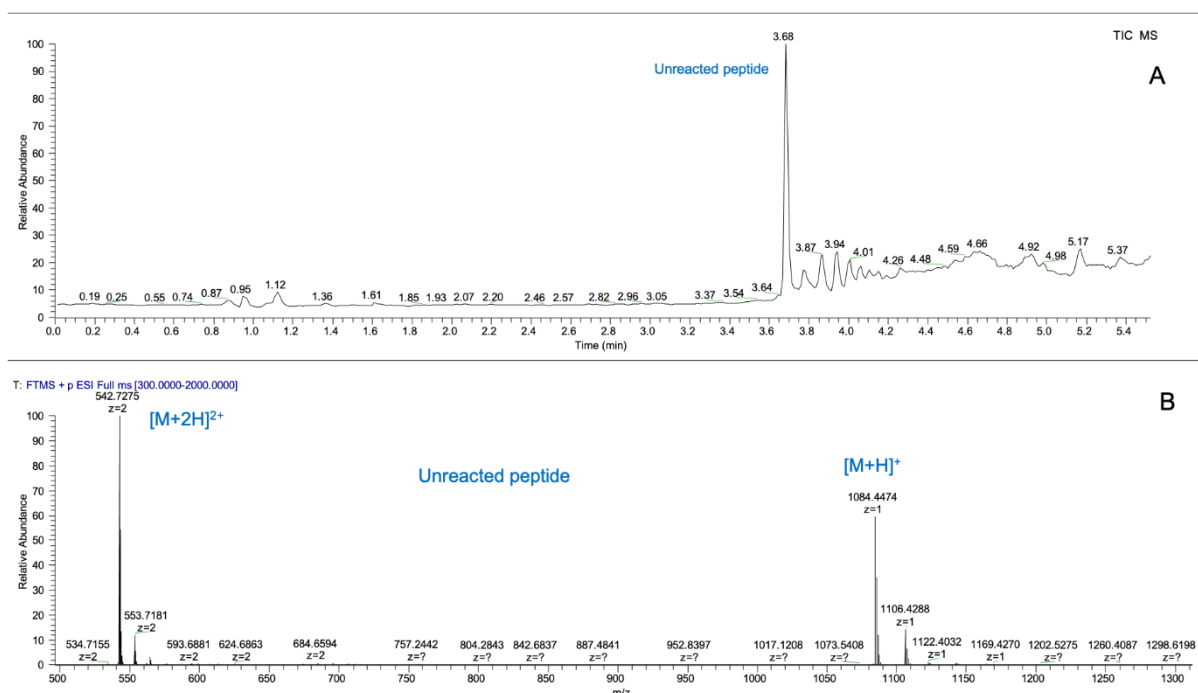


Figure S29. LC-MS of AVP incubated 18 h with Hg₂Cl₂ (3 equiv) at 37 °C in presence of DTT. **(A)** TIC. **(B)** MS spectrum of peak at $t_R = 3.68$ min.

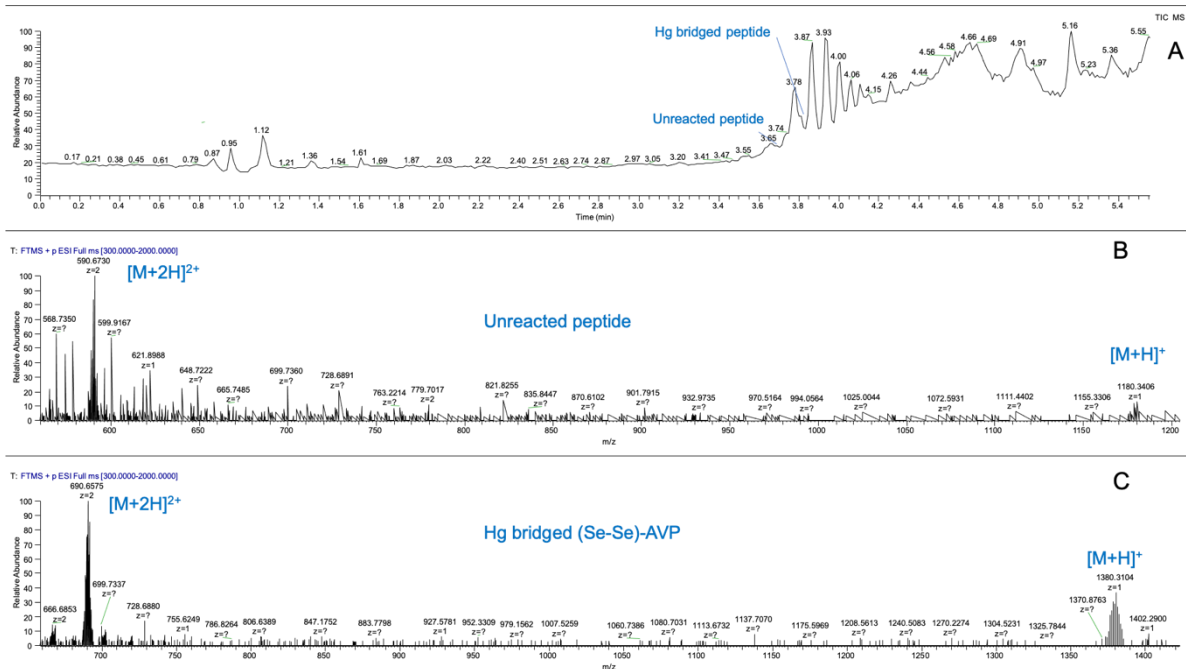


Figure S30. LC-MS of (Se-Se)-AVP incubated 18h with Hg₂Cl₂ (3 equiv) at 37°C in presence of DTT. **(A)** TIC. **(B)** MS spectrum of peak at $t_R = 3.70$ min. **(C)** MS spectrum of peak at $t_R = 3.81$ min.

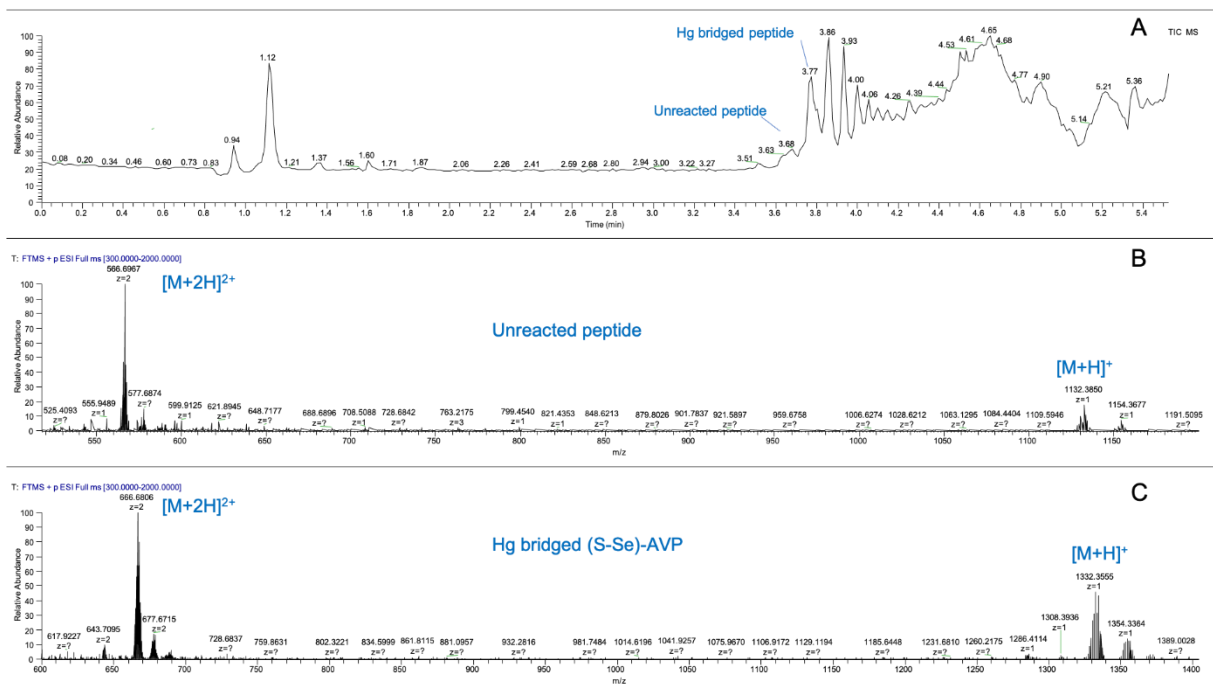


Figure S31. LC-MS of (S-Se)-AVP incubated 18h with Hg₂Cl₂ (3 equiv) at 37°C in presence of DTT. (A) TIC. (B) MS spectrum of peak at t_R = 3.69 min. (C) MS spectrum of peak at t_R = 3.79 min

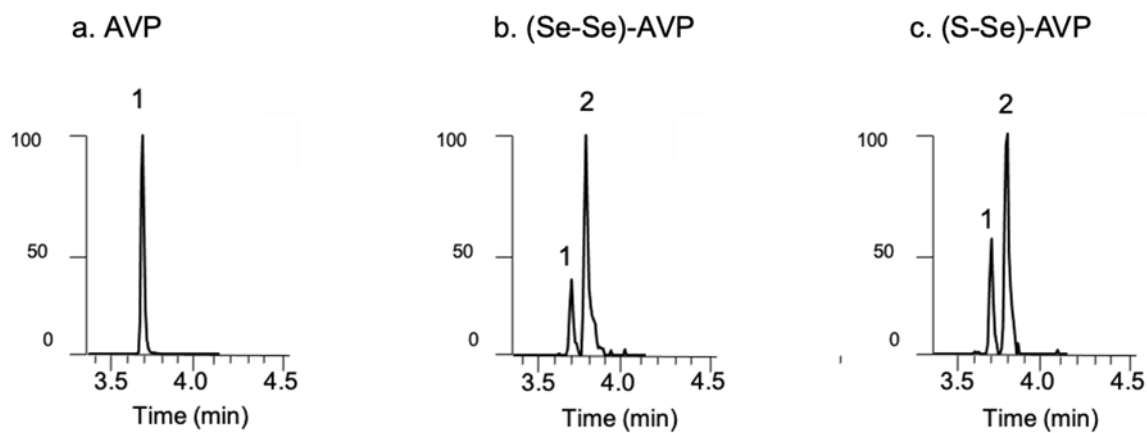


Figure S32. LC-MS of AVP peptides incubated 18 h with 3 equiv of Hg₂Cl₂ at 37 °C in presence of DTT (a) XIC of ions m/z 542.72 (AVP, t_R=3.68 min) and 643.71 (Hg-bridged AVP, t_R=3.77 min), (b) XIC of ions m/z 590.67 ((Se-Se)-AVP, t_R=3.70 min) and 690.65 (Hg-bridged (Se-Se)-AVP, t_R=3.81 min), (c) XIC of ions m/z 566.70 ((S-Se)-AVP, t_R=3.69 min) and 666.68 (Hg-bridged (S-Se)-AVP, t_R=3.79 min).

2.6. Competitive reactivity study

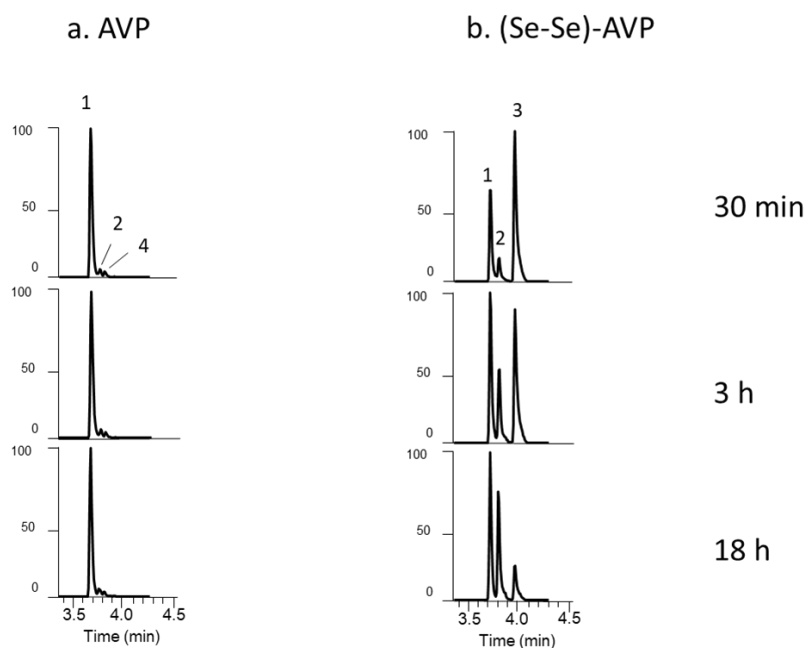


Figure S33. LC-MS of equimolar quantity of AVP (1 equiv) and (Se-Se)-AVP (1 equiv) incubated with 1 equiv of CH_3HgCl at 37 °C during 30 min, 3 h and 18 h. (a) AVP: XIC of ions m/z 542.72 (**1** AVP, $t_R=3.69$ min), 643.71 (**2** Hg-bridged AVP, $t_R=3.78$ min) and 651.72 (**4** monometallated AVP adduct, $t_R=3.87$ min), (b) (Se-Se)-AVP: XIC of ions m/z 590.67 (**1** (Se-Se)-AVP, $t_R=3.71$ min), 690.65 (**2** Hg-bridged (Se-Se)-AVP, $t_R=3.81$ min) and 805.66 (**3** bis-metallated (Se-Se)-AVP, $t_R=4.00$ min).

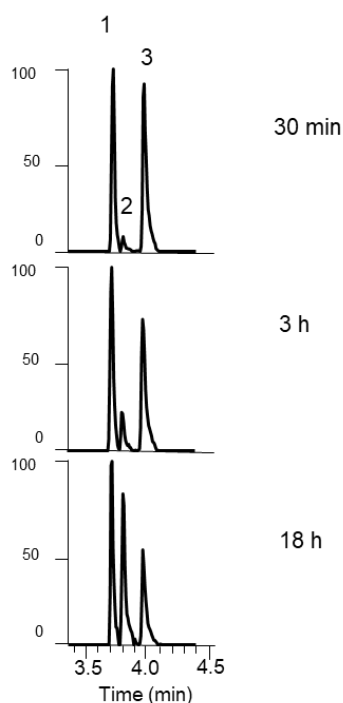


Figure S34. LC-MS of 10:1 AVP to (Se-Se)-AVP incubated with 1 equiv of CH_3HgCl at 37 °C during 30 min, 3 h and 18 h. XIC of ions m/z 590.67 (**1** (Se-Se)-AVP, $t_R=3.70$ min), 690.65 (**2** Hg-bridged (Se-Se)-AVP, $t_R=3.82$ min) and 805.66 (**3** bis-metallated (Se-Se)-AVP, $t_R=4.02$ min).

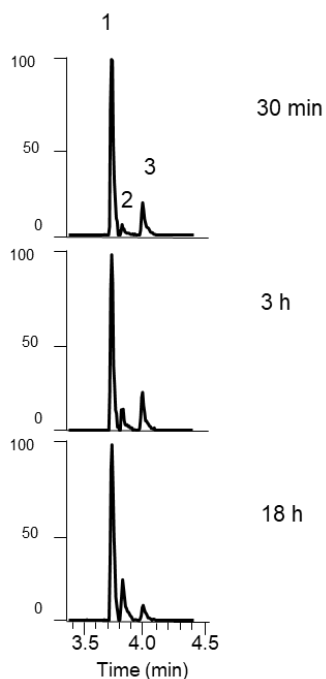


Figure S35. LC-MS of 50:1 AVP to (Se-Se)-AVP incubated with 1 equiv of CH_3HgCl at 37°C during 30 min, 3 h and 18 h. XIC of ions m/z 590.67 (**1** (Se-Se)-AVP, $t_R=3.70$ min), 690.65 (**2** Hg-bridged (Se-Se)-AVP, $t_R=3.82$ min) and 805.66 (**3** bis-metallated (Se-Se)-AVP, $t_R=4.02$).

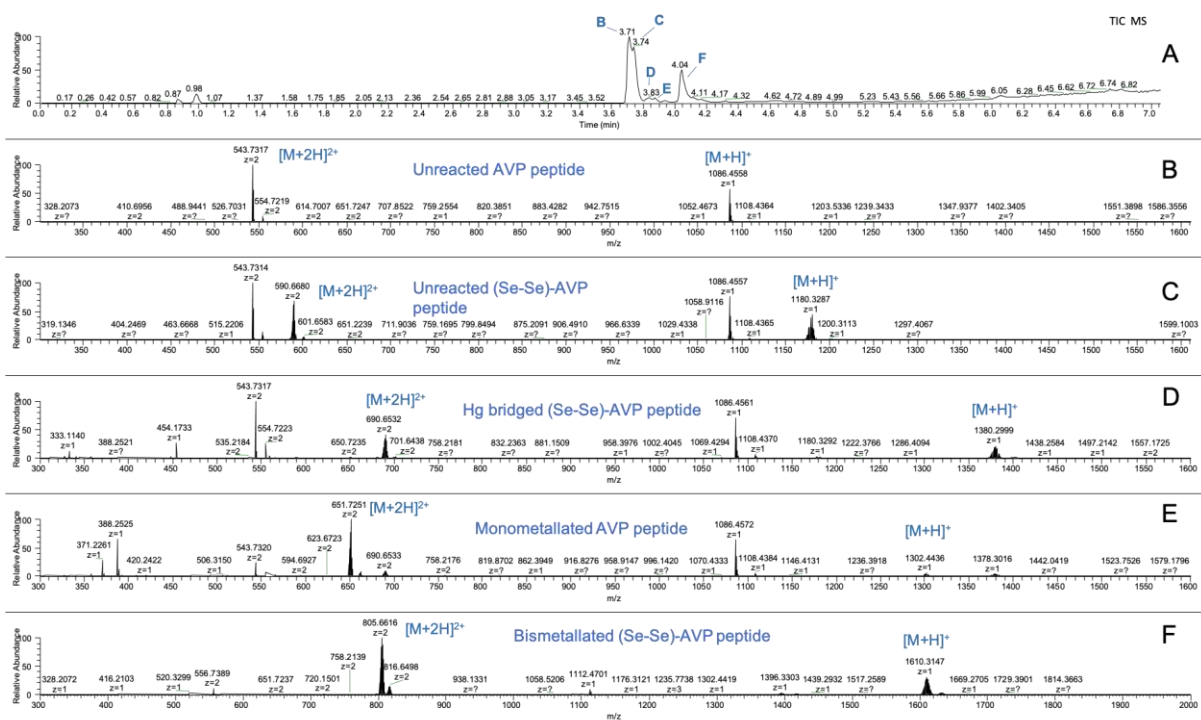


Figure S36. LC-MS of AVP (pre-treated with DTT) firstly incubated with 1 equiv of CH_3HgCl at 37°C during 18 h then reacted with 1 equiv of (Se-Se)-AVP. **(A)** TIC. **(B)** MS spectrum of peak at $t_R = 3.71$ min. **(C)** MS spectrum of peak at $t_R = 3.74$ min. **(D)** MS spectrum of peak at $t_R = 3.82$ min. **(E)** MS spectrum of peak at $t_R = 3.83$ min. **(F)** MS spectrum of peak at $t_R = 4.04$ min.

2.7. MS/MS of Hg-peptide adducts

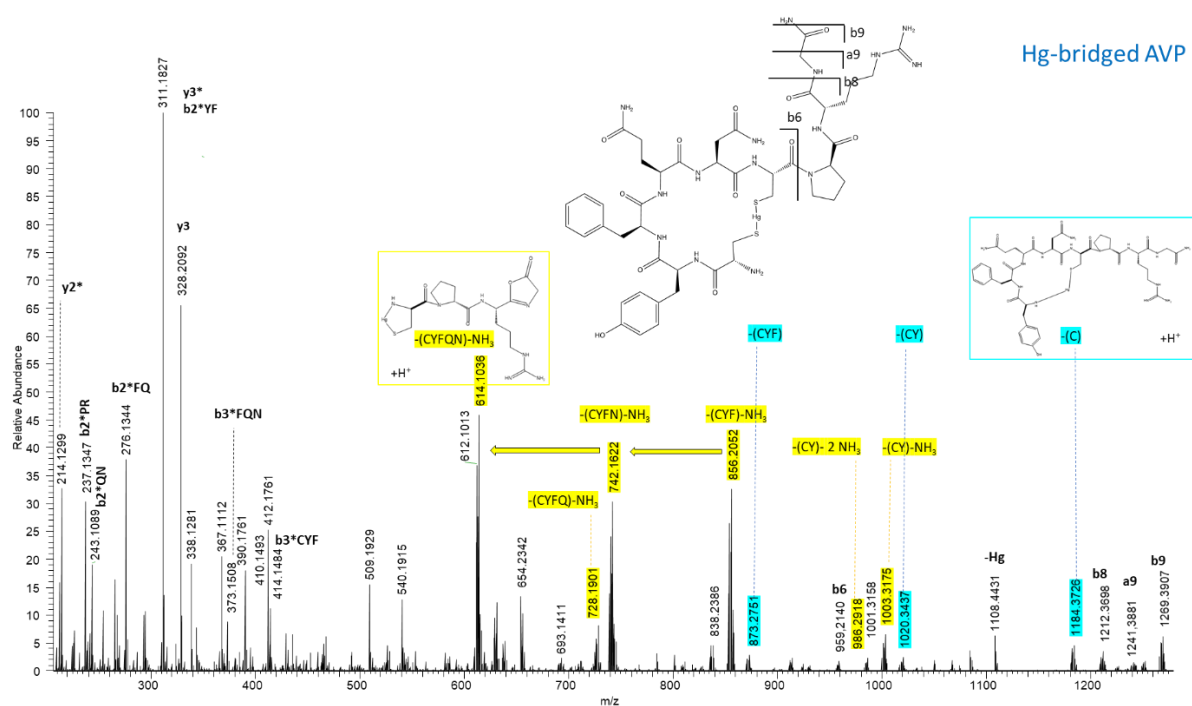


Figure S37. MS/MS of Hg-bridged AVP at m/z 1286.4126 ($z=1$). Principal fragments at HCD = 30.



Figure S38. MS/MS of bis-metallated AVP at m/z 1516.4280 ($z=1$). Principal fragments at HCD = 30.

Monometallated AVP

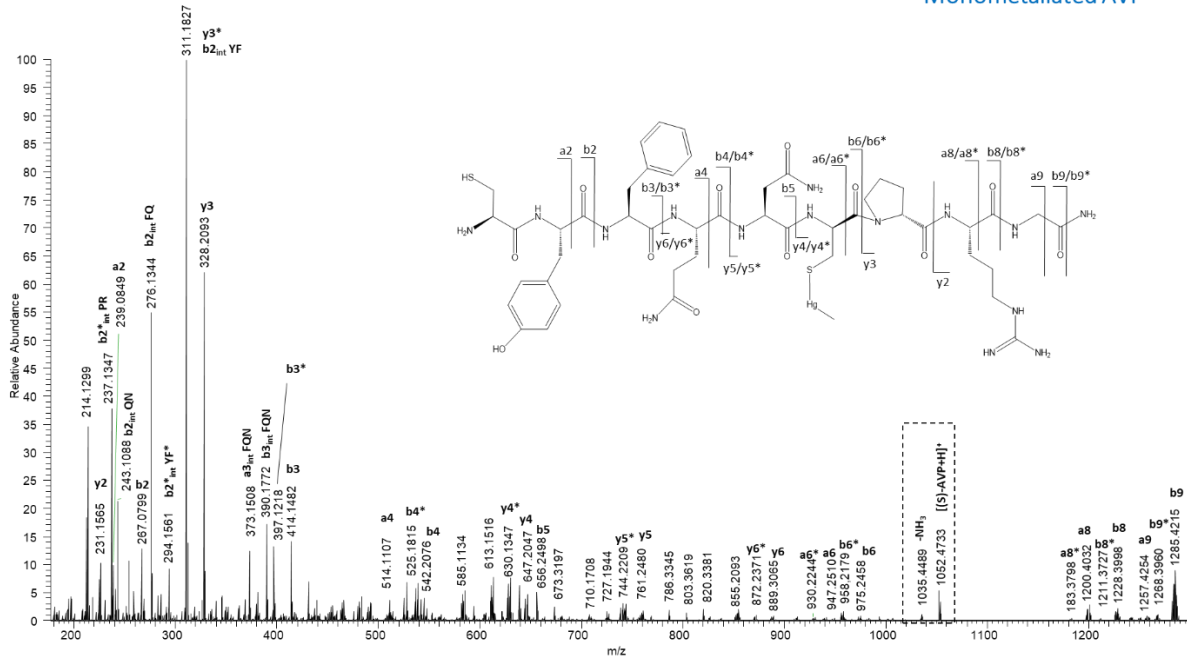


Figure S39. MS/MS of monometallated AVP at m/z 1302.4441 ($z=1$). Principal fragments at HCD = 30.

Monometallated AVP'

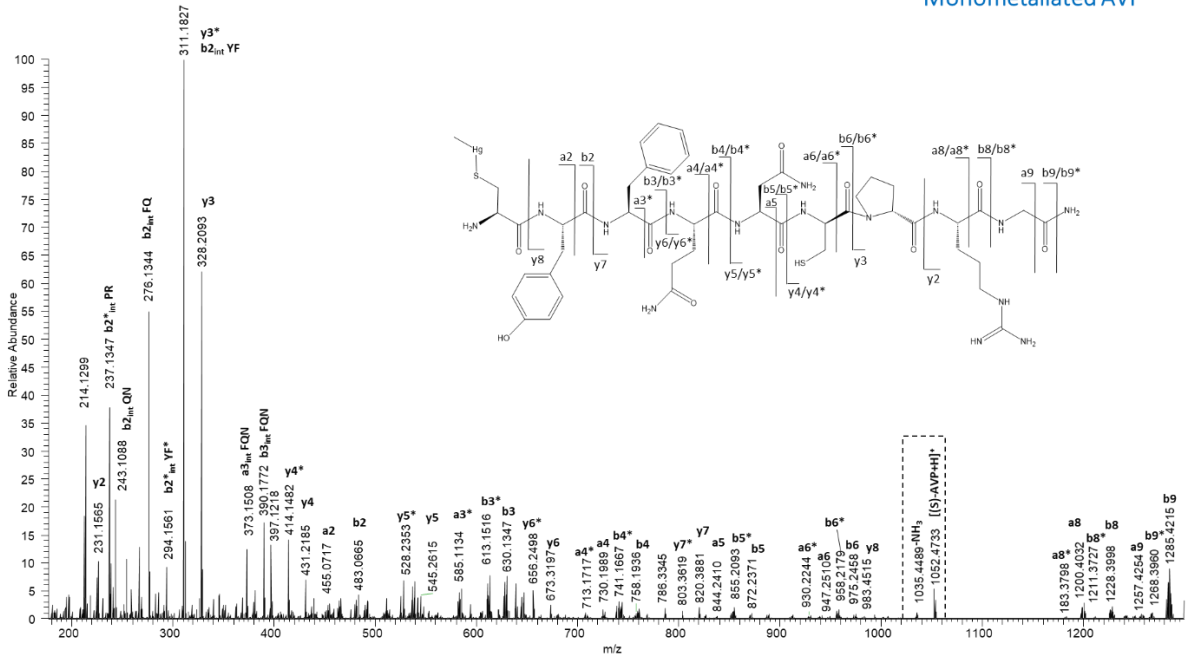


Figure S40. MS/MS of monometallated AVP' at m/z 1302.4441 ($z=1$). Principal fragments at HCD = 30.

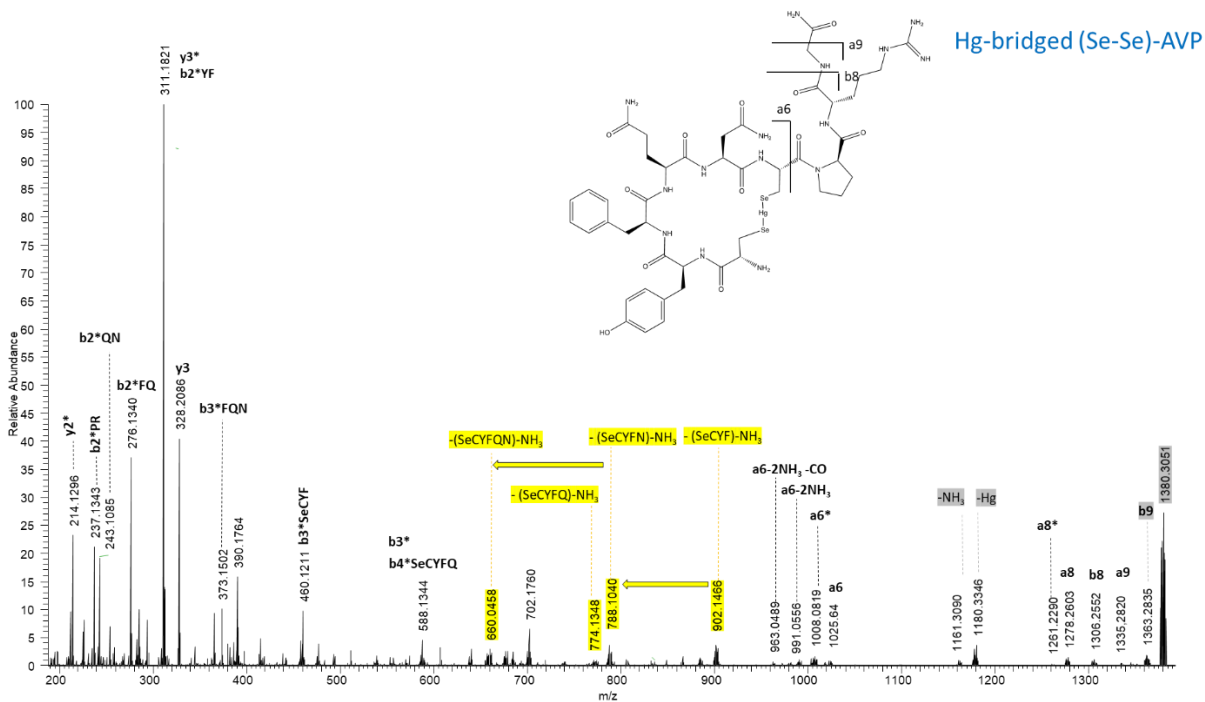


Figure S41. MS/MS of Hg-bridged (Se-Se)-AVP at m/z 1380.3044 ($z=1$). Principal fragments at HCD = 30.

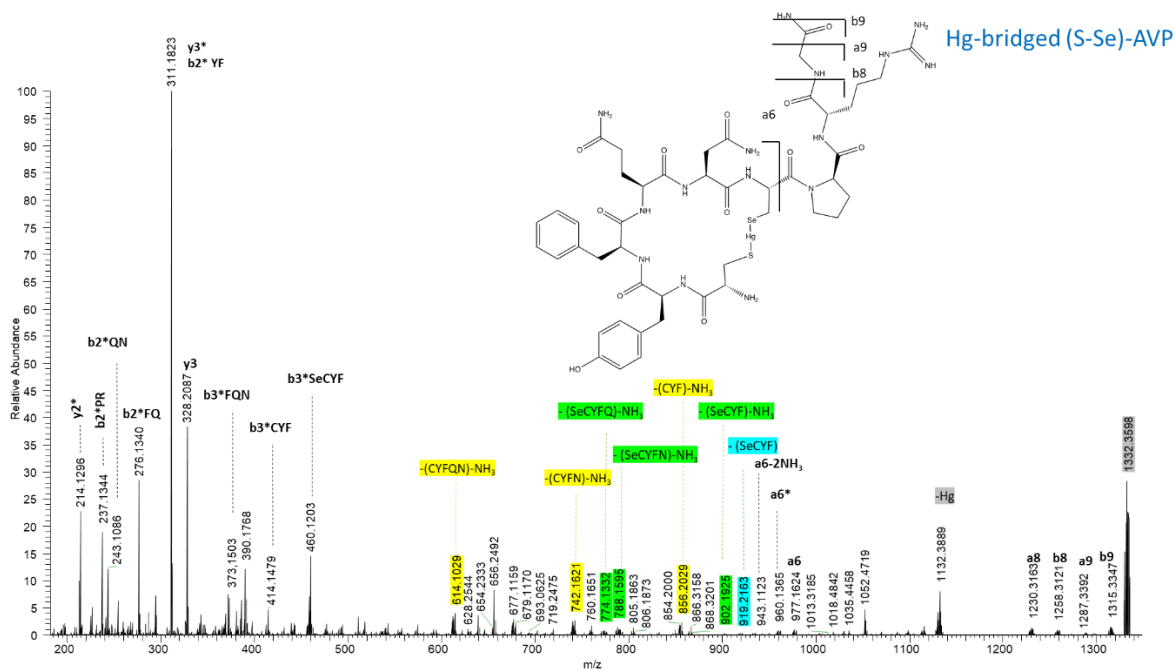


Figure S42. MS/MS of Hg-bridged (S-Se)-AVP at m/z 1332.3560 ($z=1$). Principal fragments at HCD = 30.

Bis-metallated (S-Se)-AVP

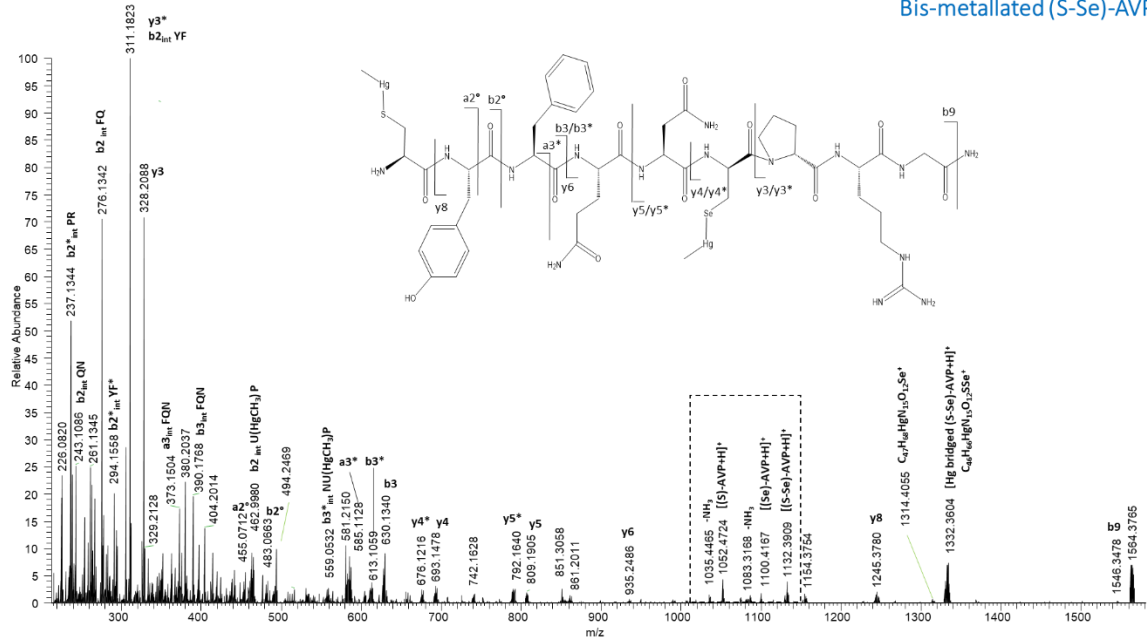


Figure S43. MS/MS of bis-metallated (S-Se)-AVP at m/z 1564.3719 ($z=1$). Principal fragments at HCD = 30.

Monometallated (S-Se)-AVP

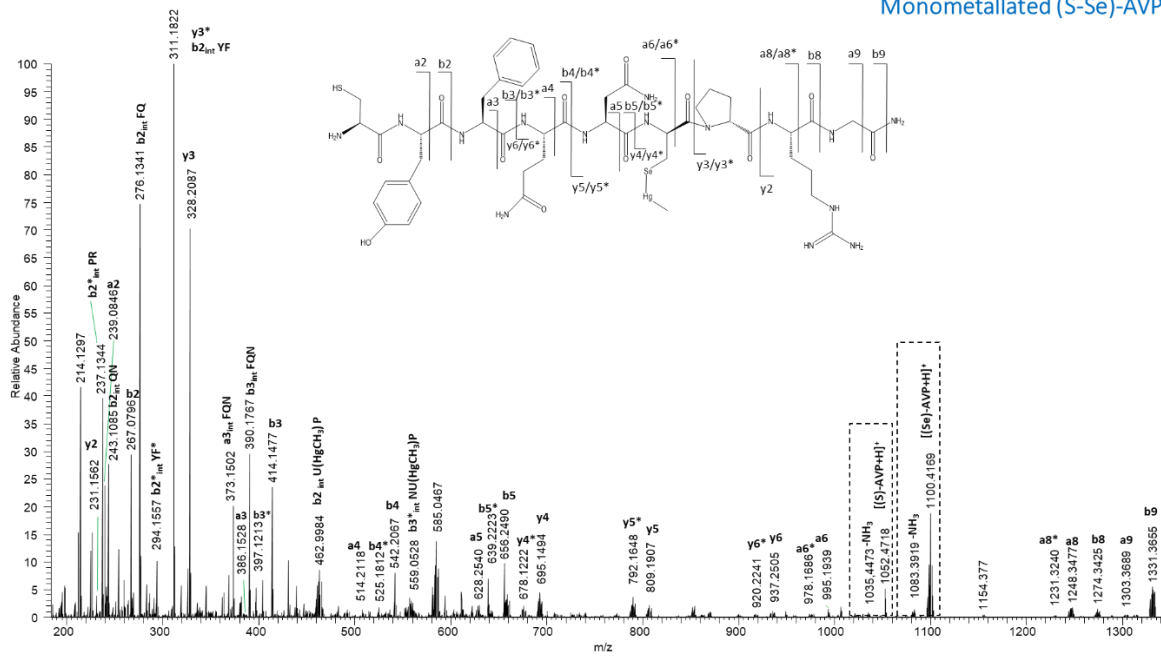


Figure S44. MS/MS of monometallated (S-Se)-AVP at m/z 1348.33860 ($z=1$). Principal fragments at HCD = 30.

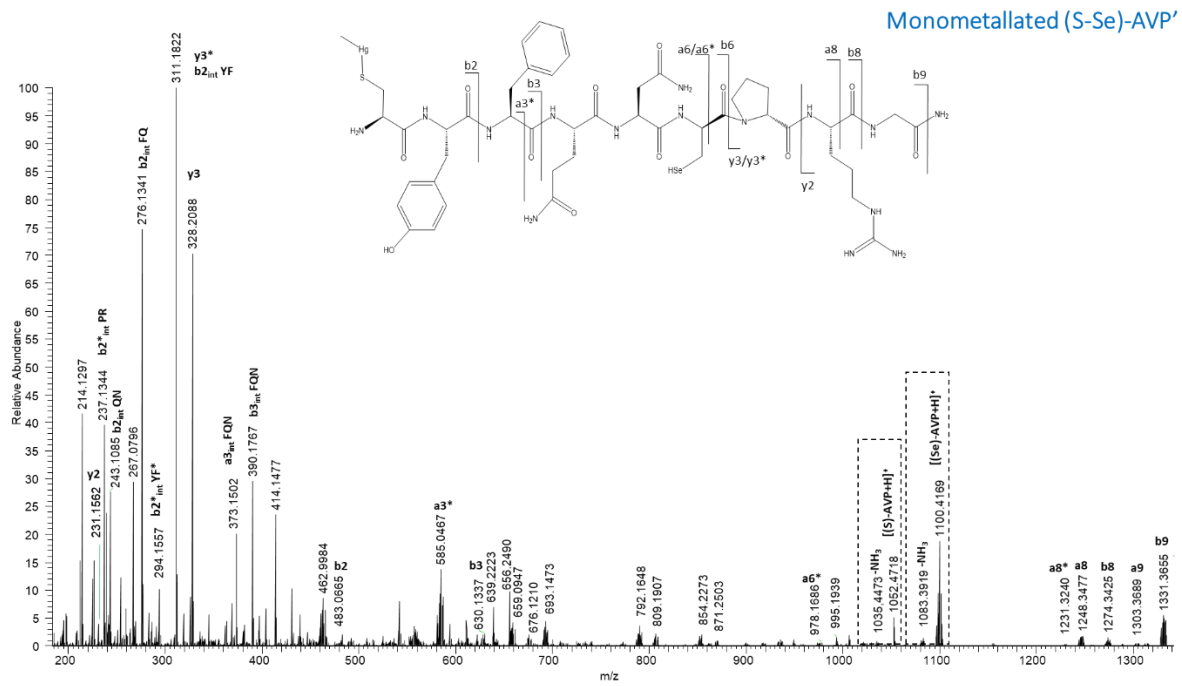


Figure S45. MS/MS of monometallated (S-Se)-AVP at m/z 1348.33860 ($z=1$). Principal fragments at HCD = 30.